RSC Advances

PAPER

View Article Online
View Journal | View Issue

Check for updates

Cite this: *RSC Adv.*, 2025, **15**, 15138

Synthesis, molecular docking, and *in vitro* activity of a novel angiotensin-converting enzyme 2 inhibitor, LMS1007: a potential molecule in Covid-19 and cancer treatments†

Loai Saadah, *[a] Ghina'a Abu Deiab, [b] Qosay Al-Balas [c] and Iman Basheti [de]

Received 16th February 2025
Accepted 22nd April 2025

DOI: 10.1039/d5ra01134e

rsc.li/rsc-advances

Angiotensin-converting enzyme 2 (ACE2) is a validated commonly studied in the pathology of several diseases, including novel coronavirus and breast cancer. Herein, we report the synthesis, molecular docking, and validation of a novel ACE2 inhibitor that was previously discovered by our team based on diverse scaffolds of other ACE2 inhibitors and carnosine. The synthesized 4-subsitituted imidazole compound, namely, **LMS1007**, was characterized through ^{1}H-NMR, LC-MS, and SFC. **LMS1007** was then tested *in vitro* with ACE2 and viral spike protein–ACE2 inhibitor kits and was found to be approximately 100 times more potent as an ACE2 inhibitor than carnosine. However, it was less potent than the standard ACE2 inhibitor. In the same concentration range of the standard drug for ACE2 inhibition, **LMS1007** demonstrated similar inhibitory effects on the interaction of the viral spike protein with ACE2. **LMS1007** had an inhibitory concentration of 50% (IC_{50}) at a concentration of 2.3 mM in all kits. **LMS1007**, similar to carnosine in breast cancer cell lines, exhibited potential inhibitory effects on the ACE2-mediated host uptake of Covid-19. Thus, a thorough review and discussion are provided on the role of ACE2 as an attractive target for the development of new drugs for Covid-19 treatment.

Open Access Article. Published on 08 May 2025. Downloaded on 2/10/2026 7:24:35 PM.
This article is licensed under a Creative Commons Attribution-NonCommercial 3.0 Unported Licence.

Introduction

Angiotensin-converting enzyme 2 (ACE2) has emerged as a pivotal molecular mediator in diverse pathological processes, notably including Covid-19 and breast cancer.[1] The host's ACE2 receptor facilitates viral entry by binding to the viral spike glycoprotein, thereby enabling viral internalization into host cells.[2] Interestingly, the modulation of ACE2 activity presents a viable therapeutic strategy to disrupt this critical viral–host interaction. For example, ACE2 downregulation has a protective effect against severe acute respiratory syndrome coronavirus 2 (SARS CoV-2) in cystic fibrosis patients.[3] Additionally, allosteric changes that are induced by heparin facilitate ACE2–spike protein binding and viral entry.[4]

Carnosine, a naturally occurring supplement, stands out in virtual screening and *in silico* studies as a potential ACE2 inhibitor, underpinning its broad-spectrum pharmacological efficacy (Fig. 1A).[5] One of our research teams substantiated this hypothesis in an experimental seminal study.[6] Therein, carnosine had shown both ACE2 and triple negative breast cancer (TNBC) cell line proliferation inhibition at the same concentration range. The IC_{50} value of carnosine for ACE2 activity inhibition and the anti-proliferative effect was in the range of 100–300 mM. This constituted the first time that ACE2 inhibition and the antiproliferative effect were presented as a coupled effect. However, it is not clear whether ACE2 inhibition would have positive implications for SARS CoV-2 replication as it did for TNBC cell line proliferation. In this same study, MCF-7 proliferation increased but non-significantly in the 100–300 mM range. This contrasts with two other research groups that have shown that the antiproliferative effect of carnosine is associated with an IC_{50} value of about 68 mM.[7] In this range,[8] it has been shown that carnosine reduces the breast cancer tumor size in mice. Moreover, emerging research shows that various drugs interacting with the ACE2/Ang1-7/Mas and ACE/AngII/AT1 axes affect their anticancer properties.[9] Therefore, further studies in this area may help elaborate on the role of ACE2 inhibition in various diseases and cell lines.

Collaterally, an international patent has been previously registered by our research group for 25 novel substituted imidazole-based compounds that have been computationally predicted as

[a]*Faculty of Pharmacy, Applied Science Private University, 11937 Amman, Jordan. E-mail: l_saadah@asu.edu.jo; Tel: +962798222044*

[b]*Faculty of Pharmacy, Yarmouk University, 21163 Irbid, Jordan. E-mail: ghinaadeiab@gmail.com; Tel: +962791101303*

[c]*Faculty of Pharmacy, Jordan University for Science & Technology, 22110 Irbid, Jordan. E-mail: qabalas@just.edu.jo; Tel: +962776337216*

[d]*Faculty of Pharmacy, Jadara University, 21110 Irbid, Jordan. E-mail: i.basheti@jadara.edu.jo; Tel: +962797708060*

[e]*Faculty of Medicine and Health, School of Pharmacy, The University of Sydney, 2006 NSW, Australia*

† Electronic supplementary information (ESI) available. See DOI: https://doi.org/10.1039/d5ra01134e

© 2025 The Author(s). Published by the Royal Society of Chemistry

Open Access Article. Published on 08 May 2025. Downloaded on 2/10/2026 7:24:35 PM.
This article is licensed under a Creative Commons Attribution-NonCommercial 3.0 Unported Licence.

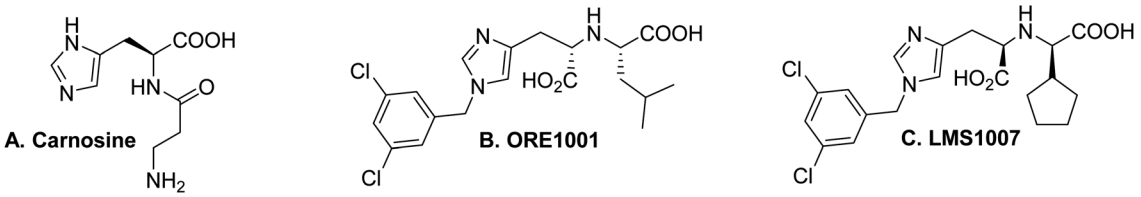

Fig. 1 Structures of (A) Carnosine, (B) ORE1001, and (C) **LMS1007**.

potential ACE2 inhibitors.[10] The compounds have been designed and studied *in silico*, resulting in a lower Gibbs free energy when docked with ACE2. The results indicated that the compounds have higher affinity and ACE2 inhibition than carnosine and ORE1001 (also known as MLN-4760), another standard ACE2 inhibitor (Fig. 1B). Pharmacokinetic predictor tools have shown that some of these compounds have drug-like properties. Therefore, in this review, we report the detailed docking, chemical modeling, chemical synthesis, characterization, and experimental validation of one of the compounds, namely **LMS1007** (Fig. 1C). For the complete structures of all 25 compounds that were docked, please refer to our international patent.[10]

The present review aims to achieve four main objectives. First, a comprehensive molecular docking and chemical modeling of the novel compounds are presented to identify the most promising candidate for synthesis. Second, **LMS1007** has been synthesized and characterized. Third, experimental validation of the **LMS1007** inhibitory activity against ACE2 and viral spike protein–ACE2 binding has been reported. Finally, the most current literature on the topic is discussed to further emphasize the need for more research on ACE2 in Covid-19, as well as other diseases. The research hypotheses, derived from prior studies, posit the following:

LMS1007 will exhibit superior or more potent ACE2 inhibitory activity compared to carnosine.

LMS1007 will effectively inhibit ACE2 and its interaction with the Covid-19 spike protein within the same concentration range.

Methods

Detailed docking and chemical modeling

Protein selection and preparation. The crystal structure of the targeted protein "SARS-CoV-2 spike receptor-binding domain bound with ACE2" has been downloaded from the Protein Data Bank (PDB: 6 M0J).[11] SARS-CoV-2 is a *Homo sapiens* protein with a resolution of 2.45 Å. The structure was prepared using Discovery Studio 2022 (DS 2022) software from BioVia® (BIOVIA, Dassault Systèmes, Discover Studio 2022, San Diego: Dassault Systèmes [2022]). The protein was subjected to a series of refinements to make sure that there were no defects in the subsequent steps. Protein preparation was executed using "Prepare Protein" protocol by which modeler inserts missing loops if present to the protein, then it was refined by Looper *via* CHARMm minimization. The protonation step was performed, wherein the titratable amino acids were protonated according to the physiological pH values and positioning hydrogen appropriately.

Protein minimization. The resulting protein structure from the preparation step was subjected to a refinement step that is critical for securing proper docking conditions. Minimization of the protein relaxed any strained structures within the protein that resulted from the crystallization step, to properly position the atoms with a suitable force field application. This step was crucial as the deformities of the targeted protein were resolved.

The minimization steps were as follows; first, the protein was solvated with water to mimic its natural environment using the "solvation" protocol. An explicit periodic boundary was selected to solve the protein with the periodic boundary conditions. Then, counterions were added to help keep the system neutral with a desirable value. The second step involved the minimization stage, which was successfully accomplished *via* three steps by avoiding any deformed structures of the protein. (1) The protein backbone and side chains were fixed by applying harmonic strain within the first minimization. Only the water molecules and the hydrogens of the protein were allowed to move. Smart minimizer was applied, as the starting structure is expected to be poor. Within it, the steepest descend protocol was applied to a gradient RMS of 3, and then a conjugate gradient protocol was applied to reach an acceptable energy minimized structure. (2) The backbone of the protein was fixed, and the side chains with the rest of the system were allowed to move and resonate with the same smart minimizer protocol. (3) The system was allowed to completely move without restrictions by using the same smart minimizer protocol. Finally, the water molecules, ions and counterions were removed from the system. The protein was ready for the subsequent steps of ligand docking.

Defining the active sites. The active site determination was a crucial step in this work. Discovery Studio 2022 (DS 2022) (software from BioVia® (BIOVIA, Dassault Systèmes, Discover Studio 2022, San Diego: Dassault Systèmes [2022])) was utilized to define the active site in this step. The targeted area within this work was large as it expanded along the two protein interaction surfaces. In addition, the exact active site was difficult to attain as the contact area between the two proteins was largely extended. The strategy followed in choosing the docking site within the two proteins interfaces (spike and ACE2) involved the application of a distance monitor that detected the areas of contact with the smallest distances between the two proteins. The key amino acids that are in close proximity to each other within the two proteins were considered the base for choosing the docking sphere for the active site. Herein, a distance monitor of 3 Å was applied between the spike and the ACE2 proteins. Three nearest contact areas were discovered, and the three active sites were assigned by choosing the amino acid as the center of the docking sphere for docking along the border areas of the two enzymes. The selected amino acids chosen for active site determination in the two proteins are reported in the results section. Amino acids

Open Access Article. Published on 08 May 2025. Downloaded on 2/10/2026 7:24:35 PM. This article is licensed under a Creative Commons Attribution-NonCommercial 3.0 Unported Licence.

are better identifiers here since the coordinates are varied in PDB proteins and could be different from those determined based on selected amino acids. The docking sphere in which the docked compounds can be positioned freely was between 9.9–10 Å to give the full potential of active site discovery.

Ligands' preparation. The designed 25 ligands were drawn using ChemDraw software, and then transferred to DS 2022 in preparation for the docking step. The ligands were prepared using "ligand preparation" protocol, in which the ionization was applied at a pH range of 6.5–8.5, resembling the physiological conditions. Canonical tautomers were generated for the ligands to make sure the chemical space was covered. In addition, isomers were generated for all chiral atoms as the stereochemistry of the original designed ligands was not determined, leaving the molecular modeling study to decide the optimum isomer for enzyme binding. Collectively, 260 ligands were generated and docked to find the suitable hit compounds.

Docking. LibDock protocol was used, which is characterized by docking the ligands inside the active site using hotspots. Ligand conformations were aligned to polar and nonpolar receptor interactions. Within this protocol, the minimization steps were performed to optimize the interactions with the active site and to give suitable scoring parameters. The 260 ligands were docked using the most computationally extensive parameters to get the best conformations and best poses. The modest number of ligands used here enabled us to perform the most accurate parameters, as this was achieved in a reasonable time. The resulting LibDock Score was used as an evaluating parameter for the best ligand and best pose.

Experimental chemistry

General information. LMS1007 was custom synthesized by BOC Sciences company with >95% purity, as determined by liquid chromatograph mass spectra (LC-MS) and >95% purity diastereomer by supercritical fluid chromatography (SFC). All reactions were performed in oven-dried glassware under anhydrous conditions and a nitrogen atmosphere. ^{1}H-NMR spectra were recorded in deuterated chloroform ($CDCl_3$), dimethyl sulfoxide (DMSO-d_6), or methanol (methanol-d_4) using a Bruker 400 spectrometer. Chemical shifts were reported in parts per million (ppm) relative to the residual deuterated solvent as an internal reference. Coupling constants, J, were reported in hertz (Hz) and multiplicities were listed as singlet (s), doublet (d), triplet (t), quartet (q), multiplet (m), *etc.* LC-MS were acquired on an Agilent LC-MS spectrometer. Thin-layer chromatography (TLC) was performed using silica gel plates 60 F_{254}.

Synthesis of benzyl D-histidinate, **2.**

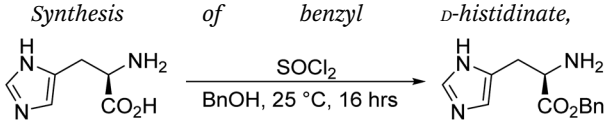

1 **2**

To a solution of compound **1** (100.0 g, 644.0 mmol) in 250.0 mL BnOH, $SOCl_2$ (60.8 mL, 837.9 mmol) was added dropwise at 0 °C. The mixture was stirred at 25 °C for 16 h. The reaction was monitored by TLC (dichloromethane/methanol = 5/1, reactant R_f = 0.08) until a new spot of compound **2** appeared. The reaction mixture was concentrated under reduced pressure, resulting in the crude product (230.5 g) as a white solid. Compound **2** was used in the next step without further purification. ^{1}H NMR: (400 MHz, DMSO-d_6) δ = 8.39 (s, 1H), 7.32–7.31 (m, 4H), 7.25–7.21 (m, 2H), 4.49 (s, 2H), 4.07 (t, J = 6.4 Hz, 1H), 3.21–3.09 (m, 2H).

Synthesis of tert-butyl (R)-4-(3-(benzyloxy)-2-((tert-butoxycarbonyl)amino)-3-oxopropyl)-1H-imidazole-1-carboxylate, **3.**

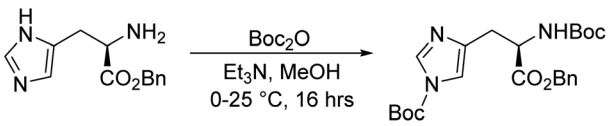

2 **3**

To a solution of compound **2** (230.5 g, 939.0 mmol) in 4600.0 mL methanol, Et_3N (183.0 mL, 1.32 mol) and Boc_2O (539.0 mL, 2.35 mol) were added dropwise at 0 °C. The mixture was stirred at 25 °C for 16 h. The reaction was monitored by TLC (petroleum ether/ethyl acetate = 3/1, reactant R_f = 0.11, product R_f = 0.66) until compound **2** was completely consumed, and three new spots with lower polarity were detected. The reaction mixture was concentrated under reduced pressure to give a residue. The residue was purified using column chromatography (SiO_2, petroleum ether/ethyl acetate = 100/1 to 10/1), resulting in the crude product of compound **3** (22.5 g, 50.5 mmol) as a white solid.

Synthesis of benzyl (tert-butoxycarbonyl)-D-histidinate, **4.**

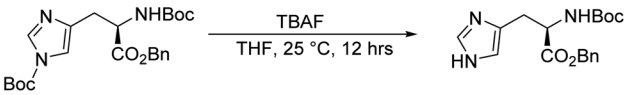

3 **4**

To a solution of compound **3** (22.5 g, 50.5 mmol) in 225.0 mL tetrahydrofuran (THF) was added TBAF (27.7 mL, 101.0 mmol) dropwise at 25 °C. Then, the mixture was stirred at 25 °C for 16 h. LC-MS showed that compound **3** was completely consumed, resulting in compound **4**. The reaction mixture was concentrated under reduced pressure to give a residue. The residue was purified by column chromatography (SiO_2, petroleum ether/ethyl acetate = 100/1 to 10/1), resulting in compound **4** (12.8 g, 37.0 mmol, 23.7% yield) as a yellow solid. ^{1}HNMR: (400 MHz, $CDCl_3$) δ = 7.45 (s, 1H), 7.30–7.23 (m, 5H), 6.72 (s, 1H), 5.71 (br s, 1H), 4.46 (br s, 1H), 3.02 (br d, J = 4.1 Hz, 2H), 2.76–2.71 (m, 1H), 1.36 (s, 9H).

Synthesis of benzyl N^{α}-(tert-butoxycarbonyl)-N^{τ}-(3,5-dichlorobenzyl)-D-histidinate, **6.**

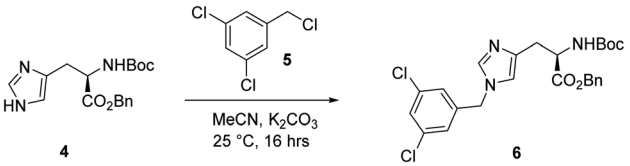

4 **6**

To a solution of compound **4** (10.0 g, 28.9 mmol) in 100.0 mL MeCN, compound **5** (11.3 g, 57.9 mmol) and K_2CO_3 (24.0 g, 173.0 mmol) were added at 25 °C. The resulting mixture was stirred at the same temperature for 16 h. LC-MS showed that compound **4** was completely consumed and ~13% desired mass was detected. The reaction mixture was filtered and concentrated under reduced pressure to give a residue. The residue was purified by column chromatography (SiO_2, petroleum ether/

© 2025 The Author(s). Published by the Royal Society of Chemistry

Open Access Article. Published on 08 May 2025. Downloaded on 2/10/2026 7:24:35 PM.
This article is licensed under a Creative Commons Attribution-NonCommercial 3.0 Unported Licence.

ethyl acetate = 100/1 to 10/1) to result compound **6** (4.0 g, 7.9 mmol, 27.3% yield) as a yellow solid. ^{1}H NMR (400 MHz, $CDCl_3$) δ = 7.34 (s, 1H), 7.24–7.19 (m, 6H), 6.87 (s, 2H), 6.24 (br s, 1H), 5.87 (br d, J = 7.6 Hz, 1H), 5.13 (br d, J = 12.3 Hz, 1H), 4.96 (br d, J = 12.2 Hz, 1H), 4.82 (br d, J = 6.6 Hz, 2H), 4.53 (br d, J = 3.2 Hz, 1H), 3.00–2.92 (m, 2H), 1.35 (s, 9H).

Synthesis of benzyl N^{τ}-(3,5-dichlorobenzyl)-D-histidinate, 7.

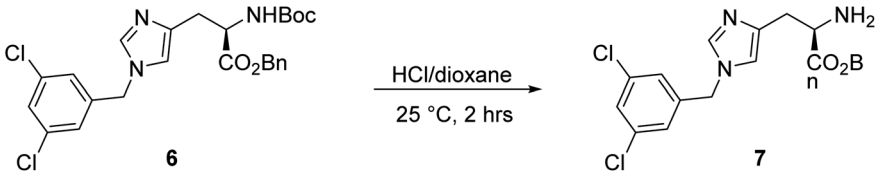

A solution of compound **6** (5.0 g, 9.9 mmol) in HCl/dioxane (4 M, 57.0 mL) was stirred at 25 °C for 2 h. LC-MS showed that compound **6** was completely consumed. The reaction mixture was concentrated under reduced pressure, diluted with 50.0 mL aqueous Na_2CO_3 and extracted with 100.0 mL dichloromethane (DCM, 50.0 mL × 2). The combined organic layers were washed with 100.0 mL aqueous NaCl (50.0 mL × 2), dried over Na_2SO_4, filtered, and concentrated under reduced pressure, resulting in the crude product. The crude product was used in the next step without further purification. Compound **7** (4.1 g, crude) was obtained as a yellow solid.

*Synthesis of benzyl N^{α}-((R)-2-(benzyloxy)-1-cyclopentyl-2-oxoethyl)-N^{τ}-(3,5-dichlorobenzyl)-D-histidinate, **9**.*

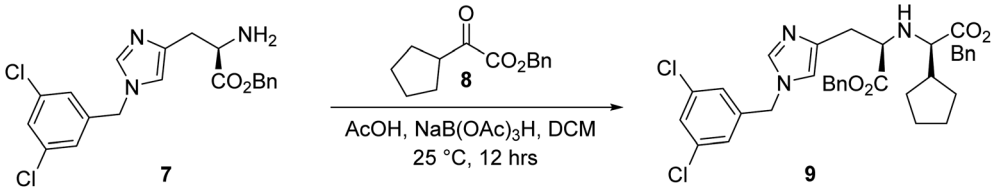

To a solution of compound **7** (2.0 g, 5.0 mmol) in 20.0 mL DCM, compound **8** (2.30 g, 9.9 mmol) and AcOH (28.3 μL, 494.0 μmol) were added at 25 °C. After 1 h, $NaB(OAc)_3H$ (3.2 g, 14.8 mmol) was slowly added. The resulting mixture was stirred at 25 °C for 16 h. LC-MS showed that compound **7** was completely consumed. Then, the mixture was adjusted to pH ~9 with 5.0 mL aqueous $NaHCO_3$, and the mixture was extracted with 5.0 mL ethyl acetate (2.0 mL × 2). The combined organic layers were washed with 4.0 mL brine (2.0 mL × 2), dried over Na_2SO_4, filtered, and concentrated under reduced pressure to give a residue. The residue was purified by column chromatography (SiO_2, petroleum ether/ethyl acetate = 100/1 to 10/1) to give the racemate product (0.8 g, 1.3 mmol, 26.0% yield) as a white solid. The racemic mixture was further separated by SFC (condition: column: DAICEL CHIRALPAK AD (250 mm × 30 mm, 10 μm); mobile phase: [CO_2-IPA (0.1% NH_3H_2O)]; B%: 0%, isocratic elution mode) to give the chiral desired compound (**9**, 0.23 g, 1.3 mmol) as a yellow oil.

*Synthesis of **LMS1007**.*

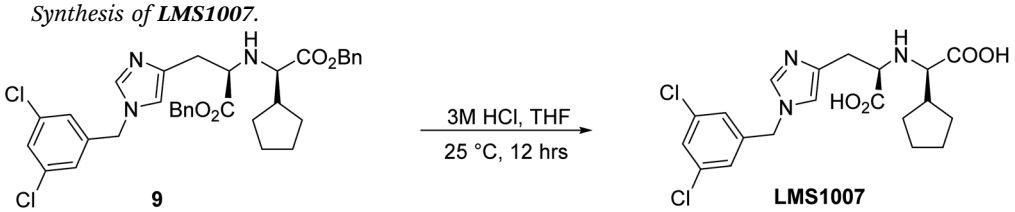

To a solution of compound **9** (0.23 g, 435.0 μmol) in 2.0 mL THF was added HCl (3 M, 1.5 mL, 10.0 eq.). The mixture was stirred at 25 °C for 16 h. The reaction was monitored by TLC (petroleum ether/ethyl acetate = 1/1, reactant R_f = 0.40, product R_f = 0.21) until compound **9** was completely consumed. The reaction mixture was filtered and concentrated under reduced pressure to give a residue. The residue was purified by prep-HPLC (column: Phenomenex Luna C18 100 × 40 mm × 3 μm; mobile phase: [H_2O (0.04% HCl)–ACN]; gradient: 15–35% B over 18.0 min). Compound **LMS1007** (23.9 mg, 53.2 μmol, 12.24% yield, 97.9% purity) was obtained as a white solid. ^{1}HNMR: (400 MHz, methanol-d_4) δ = 8.94 (s, 1H), 7.55 (t, J = 1.8 Hz, 1H), 7.52 (s, 1H), 7.43 (d, J = 1.8 Hz, 2H), 5.41 (s, 2H), 3.94 (t, J = 6.3 Hz, 1H), 3.47 (br d, J = 6.9 Hz, 1H), 3.29–3.24 (m, 2H), 2.29–2.24 (m, 1H), 1.80–1.72 (m, 2H), 1.63–1.57 (m, 4H), 1.41–1.34 (m, 2H). **LMS1007** was also checked by LC-MS and SFC. **LMS1007** was stored at −20 °C until use. **LMS1007** was prepared by dissolving different concentrations with different solvents. Amounts (≤10 mg) of **LMS1007** were dissolved in water or DMSO (11%), similar to our previous work on carnosine.

*Synthesis of 1,3-dichloro-5-(chloromethyl)benzene, **5**.*

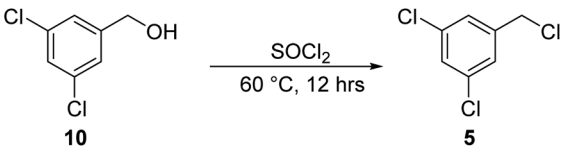

A mixture of compound **10** (10.0 g, 56.5 mmol) in 80.0 mL $SOCl_2$ was degassed, purged 3 times with N_2, and stirred at 60 °C for 12 h. The reaction was monitored by TLC (petroleum ether/ethyl acetate = 1/1, reactant R_f = 0.30, product R_f = 0.69) until compound **10** was completely consumed. The reaction mixture was concentrated under reduced pressure to give a residue. The crude product was used in the next step without further purification. Compound **5** (8 g, crude) was obtained as a yellow solid.

Open Access Article. Published on 08 May 2025. Downloaded on 2/10/2026 7:24:35 PM.
This article is licensed under a Creative Commons Attribution-NonCommercial 3.0 Unported Licence.

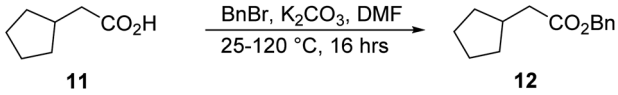

11 12. 12

A mixture of compound **11** (19.6 mL, 156.0 mmol), BnBr (18.5 mL, 156.0 mmol), and K_2CO_3 (32.4 g, 234.1 mmol) were dissolved in 160.0 mL dimethylformamide (DMF) at 25 °C. Then, the mixture was stirred at 120 °C for 16 h. The reaction was monitored by TLC (petroleum ether/ethyl acetate = 3/1, reactant $R_f = 0.31$, product $R_f = 0.65$) until compound **11** was completely consumed, and two new spots with lower polarity were detected. After completion, the reaction mixture was quenched with 100.0 mL of saturated aqueous NH_4Cl solution and extracted with 200.0 mL ethyl acetate (100.0 mL × 2). The combined organic layers were washed with 100.0 mL brine, dried over Na_2SO_4, filtered, and concentrated under reduced pressure to give a residue. The residue was purified by column chromatography (SiO_2, petroleum ether/ethyl acetate = 100/1 to 10/1), resulting in compound **12** (23.0 g, 105.4 mmol, 67.5% yield) as a yellow oil. ^{1}H NMR: (400 MHz, $CDCl_3$) δ = 7.42–7.33 (m, 5H), 5.15 (s, 2H), 2.41–2.39 (m, 2H), 2.29 (td, J = 7.6, 15.3 Hz, 1H), 1.86–1.84 (m, 2H), 1.65–1.58 (m, 4H), 1.21–1.19 (m, 2H).

Synthesis of benzyl 2-cyclopentyl-2-hydroxyacetate, ***14****.*

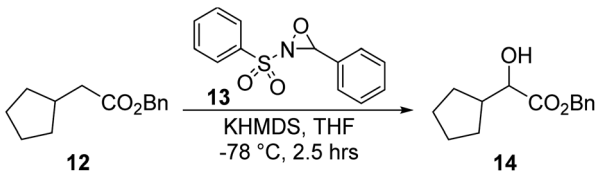

12 14

To a mixture of KHMDS (1 M, 126.0 mL, 1.2 eq.) in 100.0 mL THF, a solution of compound **12** (23.0 g, 105.4 mmol) in 100.0 mL THF was added dropwise at −78 °C. After the mixture was stirred for 30 min, a solution of compound **13** (33.0 g, 126.0 mmol) in 100.0 mL THF was added dropwise over 1 h. The reaction mixture was stirred at −78 °C for 1 h. The reaction was monitored by TLC (petroleum ether/ethyl acetate = 3/1, reactant $R_f = 0.75$, product $R_f = 0.30$) until compound **12** was completely consumed. The reaction mixture was quenched with 200.0 mL aqueous NH_4Cl and extracted with 200.0 mL diethyl ether (100.0 mL × 2). The combined organic layers were washed with 100.0 mL aqueous NaCl, dried over Na_2SO_4, filtered, and concentrated under reduced pressure to give a residue. The residue was purified by column chromatography (SiO_2, petroleum ether/ethyl acetate = 50/1 to 10/1), resulting in compound **14** (7.8 g, 33.2 mmol, 31.5% yield) as a yellow oil.

Synthesis of benzyl 2-cyclopentyl-2-oxoacetate, ***8****.*

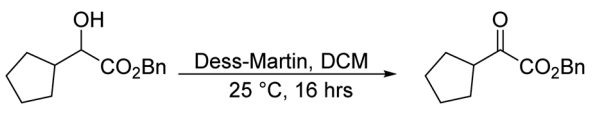

14 8

A mixture of compound **14** (7.8 g, 33.2 mmol, 1.0 eq.) and Dess–Martin (22.5 g, 53.2 mmol, 16.5 mL, 1.6 eq.) in 78.0 mL DCM was degassed, purged 3 times with N_2 gas, and stirred at 25 °C for 12 h. The reaction was monitored by TLC (petroleum ether/ethyl acetate = 8/1, reactant $R_f = 0.33$, product $R_f = 0.53$) until compound **14** was completely consumed and two new spots were formed. The reaction mixture was quenched with 100.0 mL of 10% sodium thiosulfate at 20 °C and extracted with 100.0 mL DCM (50.0 mL × 2). The combined organic layers were washed with 50.0 mL aqueous NaCl, and subsequently concentrated under reduced pressure to give a residue. The residue was purified by column chromatography (SiO_2, petroleum ether/ethyl acetate = 100/1 to 1/1) to give compound **8** (4.8 g, 20.6 mmol, 62.0% yield) as a yellow oil. ^{1}H NMR: (400 MHz, $CDCl_3$) δ = 7.31–7.27 (m, 5H), 5.20 (s, 2H), 3.45–3.37 (m, 1H), 1.80–1.74 (m, 4H), 1.57–1.59 (m, 4H).

Experimental validation of activities and hypotheses

ACE2 inhibitor screening kit. The ACE2 inhibitor screening kit (ab273373, Abcam, Boston, MA, USA) was purchased and stored in the dark at −20 °C. On the day of the experiment, the kit was thawed for 30 minutes before use. At first, a volume of 198.0 μL of ACE2 dilution buffer was introduced into the ACE2 enzyme vial. Subsequently, a working solution of ACE2 enzyme was prepared by adding 2.0 μL of the diluted ACE2 enzyme to 48.0 μL of the ACE2 assay buffer (final volume of 50.0 μL). The solution was extensively stirred; thereafter, 50.0 μL of the resultant mixture was dispensed into each of the designated wells of a 96-well microtiter plate. Following that, enzyme control (DMSO), compound **LMS1007**, and the standard kit inhibitor were formulated by dissolving the potential inhibitors in a buffer solution at concentrations of 10 (DMSO) to 100 times (**LMS1007** and the standard kit inhibitor) greater than the eventual test concentration. To attain a 10-fold dilution of the designated test concentration, the solution was diluted using assay buffer XI/ACE2. Then, 10.0 μL of the test inhibitors (**LMS1007**), standard kit inhibitor and enzyme control (DMSO) were added to each designated well, which also contained 40.0 μL substrate mix and 50.0 μL of the assay buffer. The samples underwent incubation at ambient temperature for a duration of 15 minutes before being added to the wells. A volume of 40.0 μL of the substrate mix, prepared with 2.0 μL of ACE2 substrate and 38.0 μL of assay buffer, was added to each well. The combination was fully blended; thereafter, the fluorescence intensity was observed in kinetic mode for a period of 1 hour at room temperature. Specifically, the fluorescence intensity was measured at 2, 17, 32, 47, and 62 minutes. The excitation and emission wavelengths employed were 320 nm and 420 nm, correspondingly. The slope for each well was determined by studying the linear portion of the fluorescence plot. The evaluation of ACE2 inhibition was performed across a concentration range of 23.0 nM to 23.0 mM for **LMS1007** and 6.25 nM to 50.0 nM for the standard kit inhibitor. One enzyme control set was used for both the standard kit inhibitor (quadruplet, experiment 1) and the test compound (triplicate, experiment 2). Each of the tested compounds and the kit inhibitor were compared to the enzyme control done in the same respective experiment.

LMS1007, the standard kit inhibitor, and DMSO were tested in triplicate/quadruplicate sets at up to four dilutions. For **LMS1007**, the tested concentrations included 23.0 nM, 230.0 nM, 2.3.0 μM, 23.0 μM, 230.0 μM, 2.3 mM, and 23.0 mM. The standard kit inhibitor concentrations included 6.25 nM, 12.5 nM, 25.0 nM, and 50.0 nM. For DMSO, there were up to four concentrations: 0.0625%, 0.125%, 0.25%, and 0.5%.

© 2025 The Author(s). Published by the Royal Society of Chemistry

Open Access Article. Published on 08 May 2025. Downloaded on 2/10/2026 7:24:35 PM. This article is licensed under a Creative Commons Attribution-NonCommercial 3.0 Unported Licence.

Subsequently, the activity percentage was calculated by dividing the slope of the fluorescence line for each measurement by the slope of the matching fluorescence line slope for enzyme control. Finally, the inhibition percentage was calculated for each concentration as (1 − % activity).

SARS-CoV-2 spike–ACE2 interaction inhibitor screening assay kit. The SARS-CoV-2 spike–ACE2 interaction inhibitor screening assay kit (Cayman 502050, Cayman Chemical Company, Ann Arbor, MI, USA) was purchased and stored at −20 °C. On the day of the experiment, the kit was thawed for 30 minutes before use. The pre-coated microplate was equilibrated to room temperature. Each well was washed three times with 300.0 μL of wash buffer to remove preservatives. 100.0 μL of the spike inhibitor screening reagent (SARS-CoV-2 Spike S1 RBD) was added to each well. The plate was incubated at room temperature for 1 hour on a shaker set to 300 rpm. Wells were washed three times with 300.0 μL of wash buffer. A 1 : 10 dilution of the **LMS1007** was prepared in the provided assay buffer. 50.0 μL of the **LMS1007** dilution was added to the designated wells, while 50.0 μL of the vehicle control was added to the control wells. The plate was incubated at room temperature for 30 minutes on a shaker.

50.0 μL of ACE2 inhibitor screening reagent (His-tagged ACE2 protein) was added to all wells.

The plate was incubated at room temperature for 1 hour on a shaker. Wells were washed three times with wash buffer to remove the unbound ACE2 protein. 100.0 μL of Anti-His-HRP conjugate was added to each well. The plate was incubated for 1 hour at room temperature on a shaker.

Wells were washed three times with wash buffer. 100.0 μL of TMB substrate solution was added to each well and incubated in the dark at room temperature for 10 minutes. The reaction was stopped by adding 50.0 μL of stop solution to each well. The absorbance was immediately measured at 450 nm using a microplate reader. The percent inhibition was calculated by comparing the absorbance of wells with **LMS1007** to the vehicle control wells using a similar method to the ACE2 inhibitor kit. The IC_{50} value for **LMS1007** was determined by non-linear regression analysis using similar curve fitting as well. Vehicle control wells ensured that any inhibition observed was specific to the test compound and not the assay conditions.

SARS-CoV-2 S1 protein–ACE2 binding inhibitor screening kit. The SARS-CoV-2 S1 protein–ACE2 binding inhibitor screening kit (ab283370, Abcam, Boston, MA, USA) was utilized in this experiment. On the day of the experiment, the kit was thawed for 30 minutes before use. The pre-coated microplate was equilibrated to room temperature. Each well was washed three times with 300 μL of wash buffer to remove preservatives. 100.0 μL of the spike inhibitor screening reagent (SARS-CoV-2 Spike S1 RBD) was added to each well. The plate was incubated at room temperature for 1 hour on a shaker set to 300 rpm. Wells were washed three times with 300.0 μL of Wash buffer. A 1 : 10 dilution of **LMS1007** was prepared in the provided assay buffer. 50.0 μL of the **LMS1007** dilution was added to the designated wells, while 50.0 μL of the vehicle control was added to the control wells. The plate was incubated at room temperature for 30 minutes on a shaker. 50.0 μL of ACE2 protein was added to all wells. The plate was incubated at room temperature for 1 hour on a shaker set to 300 rpm. Wells were washed three times with 300.0 μL of wash buffer to remove the unbound ACE2.

100.0 μL of HRP-conjugate was added to all wells. Then, the plate was incubated at room temperature on a shaker, followed by washing with 300.0 μL of wash buffer. 100.0 μL of the TMB substrate solution was added to each well. The wells were incubated in the dark at room temperature for 10 minutes. 50.0 μL of stop solution was added to each well to terminate the reaction. Finally, the absorbance was immediately measured at 450 nm using a microplate reader.

Percent inhibition was calculated by comparing the absorbance of wells with **LMS1007** to the vehicle control wells using a similar method to the previous two kits. The IC_{50} value for **LMS1007** was determined by non-linear regression analysis using similar curve fitting as well. Vehicle control wells ensured that any inhibition observed was specific to the test compound and not the assay conditions.

Statistical analyses. IBM SPSS Statistics 26.0 and application MyCurveFit (Beta Version, available online at URL: **https://mycurvefit.com/**, accessed Sunday June 23rd, 2024) were used. IBM SPSS Statistics (version 26.0.0.0) was used to calculate the 95% confidence interval and standard error of the mean for the triplicate/quadruplicate sets at each concentration and for each drug or solvent. For comparisons of the drugs, overlapping means and 95% confidence intervals were deemed statistically insignificant differences, whereas non-overlapping means and 95% confidence intervals were a clear proof of statistically significant difference. MyCurveFit was used to graph data and generate error bars with 95% confidence intervals (95% CI) and/or standard errors of the mean (SEM). The IC_{50} value indicated the concentration causing a 50% reduction in ACE2 activity, and was calculated from the results obtained on the MyCurveFit application. 95% CI or SEM error bars for a group mean overlapping with another group mean was reasonably considered as clear proof of statistically insignificant differences between the two ranges of concentrations for **LMS1007** and the standard kit inhibitor.

Review search strategy

The National Library of Medicine (NLM) secondary database of biomedical and life science literature (PubMed, accessed July 14th, 2024) was queried using the term (Angiotensin Converting Enzyme 2 [Title]). The filters that were used included publications in the last year, in English language, and in humans. Retrieved studies were thoroughly screened with focus on Covid-19 related papers. Our objective for the review was to summarize the current knowledge on ACE2's role in Covid-19 disease. Specifically, to determine the biological and mechanistic relations of ACE2 and Covid-19, presence of inhibitors or activators of ACE2, and the experimental proofs of biological activity of these drugs in Covid-19.

Results

Detailed docking and molecular modeling

Protein preparation and minimization. For a given Structure-Based Drug Docking (SBDD) success, the starting

Open Access Article. Published on 08 May 2025. Downloaded on 2/10/2026 7:24:35 PM.
This article is licensed under a Creative Commons Attribution-NonCommercial 3.0 Unported Licence.

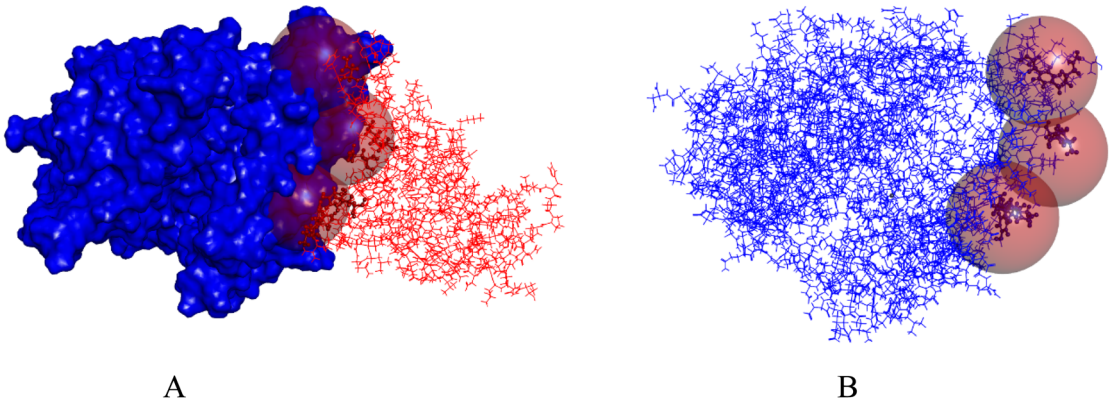

Fig. 2 (A) The ACE2 (solid blue colour) interacts with spike protein (red), and the three active spheres are assigned. (B) ACE2 receptor with its three active sites assigned at the interface.

structure should be maximally optimized. Any defects in the structure would affect the outcomes and waste time and effort. Within this work, the preparation step ensured that the starting protein structure was clean, and any missing or deformed structures were fine-tuned. The next important step was the minimization one. The strained moieties within the crystal structure were relaxed and the total energy of the system was stabilized. The final potential energy after solvation and minimization was −354 803 kcal mol^{-1} and the minimization criteria of a gradient of 0.1 was satisfied.

Active site determination. Six potential active sites within the two proteins were studied that were not previously reported in the literature. The active sites were selected based on protein surfaces analysis by measuring the distances between the proteins. Therefore, a comparative study with the active site will not be possible or applicable. Studies on the ACE2 docking are based on the defined active site with the zinc atom, and this active site is not involved in the spike–ACE2 recognition. As mentioned in the methodology section, the active site in the protein was extended over a vast area where the two proteins interacted. Thereof, three areas were assigned with an approximate radius to cover the whole contact area. The criteria used in this work for the determination of the active sites detected the close contacts between spike and the ACE2. Therefore, any amino acids that were within the range of 3 Å between the two enzymes were considered as a center of an active site sphere. ACE2 active sites were assigned with an approximate radius of 10 Å to guarantee that all of the surface was covered and to get a satisfactory docking range. The first active site with 9.9 Å was centered on TYR83 and GLN24. The second active site was based on ASP30 and LYS31 with a diameter of 9.95 Å. The third active site was assigned with a diameter of 10 Å and was based on TYR41, GLN42 and LYS 353. Fig. 2 shows the identified three ACE2 active sites. On the other hand, the three active sites of the spike protein were determined with the same criteria discussed for ACE2. The three main sites that contacted with ACE2 were determined based on the nearest amino acids. The first active site was centered on ASN487 with a 9.9 Å. Then, LYS417 and GLN493 were utilized to assign the second active site with a radius of 9.95 Å, while the last one was 10 Å, referring to amino acids GLY446, TYR449, GLY496, GLN498, THR55 and GLY502. Fig. 3 shows the identified three spike protein active sites.

Ligand preparation. Originally, 25 ligands were designed to be potential binding disrupters for ACE2–spike protein. The ligands were subjected to preparation steps to be ready for docking with all parameters and force fields assigned. Then, tautomerization, isomerization, and ionization were allowed to cover all the chemical spaces for the ligands and to ensure that all geometries were considered to identify the best isomeric forms that bind well. There were 260 resulting compounds after the preparation.

Docking using LibDock protocol. LibDock protocol for DS 2022 was employed to study the possibility of ligands to bind to the interface. The parameters of docking, as described in the methodology section, were determined to have the highest accuracy to get the best results. Six docking stages were done, with three to each receptor.

To start with, the ACE2 protein with the first active site (9.9 Å) showed no poses of any ligand, which could be explained by the inability of any ligand to bind to the active site at this position. This could be due to many reasons, such as inadequacy of the active site for binding the suggested ligands and the presence of repulsive forces that prevent proper binding. The second active site allowed for the binding of 70 ligands out of 260, with the highest scoring compound being the *S*,*S*-diastereomer of

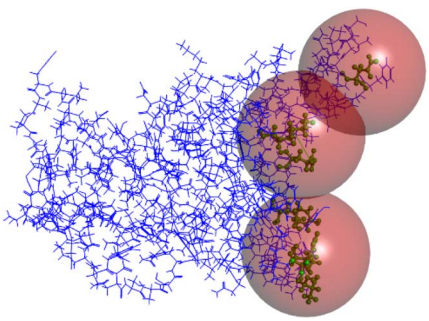

Fig. 3 The spike receptor with its three active sites assigned to the interface.

© 2025 The Author(s). Published by the Royal Society of Chemistry

Open Access Article. Published on 08 May 2025. Downloaded on 2/10/2026 7:24:35 PM.
This article is licensed under a Creative Commons Attribution-NonCommercial 3.0 Unported Licence.

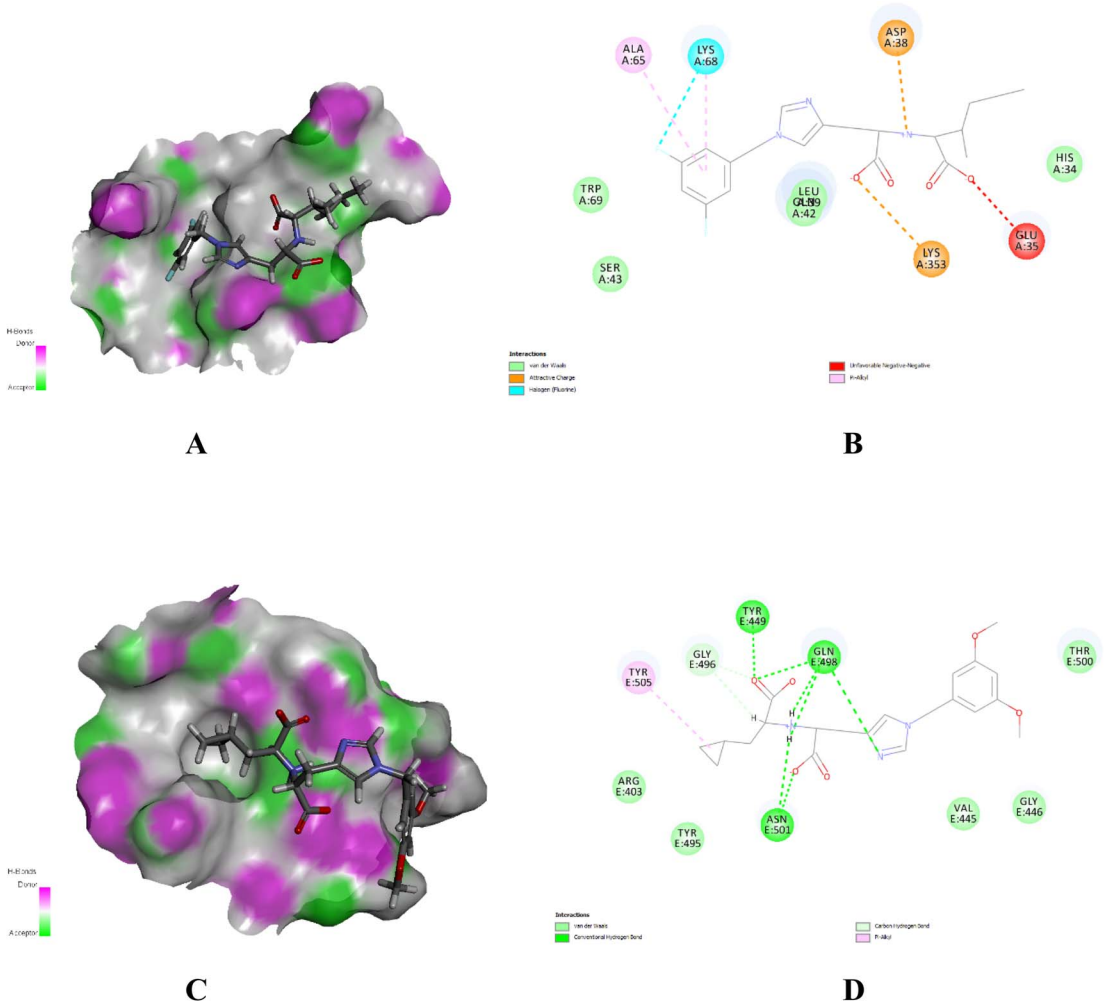

Fig. 4 (A) 3D view of compound LMS1023SSS bound in its active site with a surrounding surface showing the H-donor (purple) and H-acceptor areas (green). (B) 2D view of LMS1023SSS within the active site, showing its interactions with the amino acids at the ACE2 surface. (C) 3D view of compound LMS004RS bound in its active site with a surrounding surface showing the H-donor (purple) and H-acceptor areas (green). (D) 2D view of LMS1004RS within the active site, showing its interactions with the amino acids at the spike surface.

LMS1004 with a LibDock score value of 106.0. The third active site was the best of the three to have ligands bound to it, in which all 260 compounds had returned with docking scores. The highest score was related to the *S*,*S*,*S*-diastereomer of **LMS1023**, with a score of 105.3, while the *S*,*S*,*R*-diastereomer of **LMS1025** was in the second rank with a score of 104.8. It can be pointed out from Fig. 4, panels A and B, that one of the carboxylic acid groups of the *S*,*S*,*S*-diastereomer of **LMS1023** performs ionic interaction with the amino acids LYS353, while the other carboxylic acid shows unfavorable repulsive interactions with GLU35. The terminal hydrophobic side chain does not have any hydrophobic interactions. Similarly, the central imidazole ring does not have any interactions. The benzene ring interacts with the active site with hydrophobic interactions, while the fluorine atoms in it interact with LYS68.

Then, the spike protein (9.9 Å) was employed for docking the assigned ligands and the results were like those of the ACE2 active site (9.9 Å) with zero compounds managing to bind to the surface of the protein. Subsequently, the 9.95 Å active site was docked with the same parameters that were used in every docking trial, and only 27 ligands were able to dock within this area. The highest compound, the *R*,*R*-diastereomer of **LMS008** scored only 80.5. The third active site behaved in the same way as the ACE2 surface, and achieved the highest number of compounds to fit within it. Still, only 38 compounds have managed to bind to this site, where the *R*,*S*-diastereomer of **LMS1004** scored the highest with a LibDock score of 97.3. The interaction plot of the *R*,*S*-diastereomer of **LMS1004** can be seen in Fig. 4, panels C and D. The two carboxylic acid groups participated in binding with the active site. However, their interactions are limited to H-donor and H-acceptor. As there are no ionizable counterparts, they perform ion–dipole interactions with ASN501 and H-bonding with TYR449 and ALN498. In addition, a hydrophobic interaction is detected at the hydrophobic aliphatic cyclopropyl chain of the compound. Methoxy groups at the benzene ring have not shown any participation with the receptor.

Open Access Article. Published on 08 May 2025. Downloaded on 2/10/2026 7:24:35 PM.
This article is licensed under a Creative Commons Attribution-NonCommercial 3.0 Unported Licence.

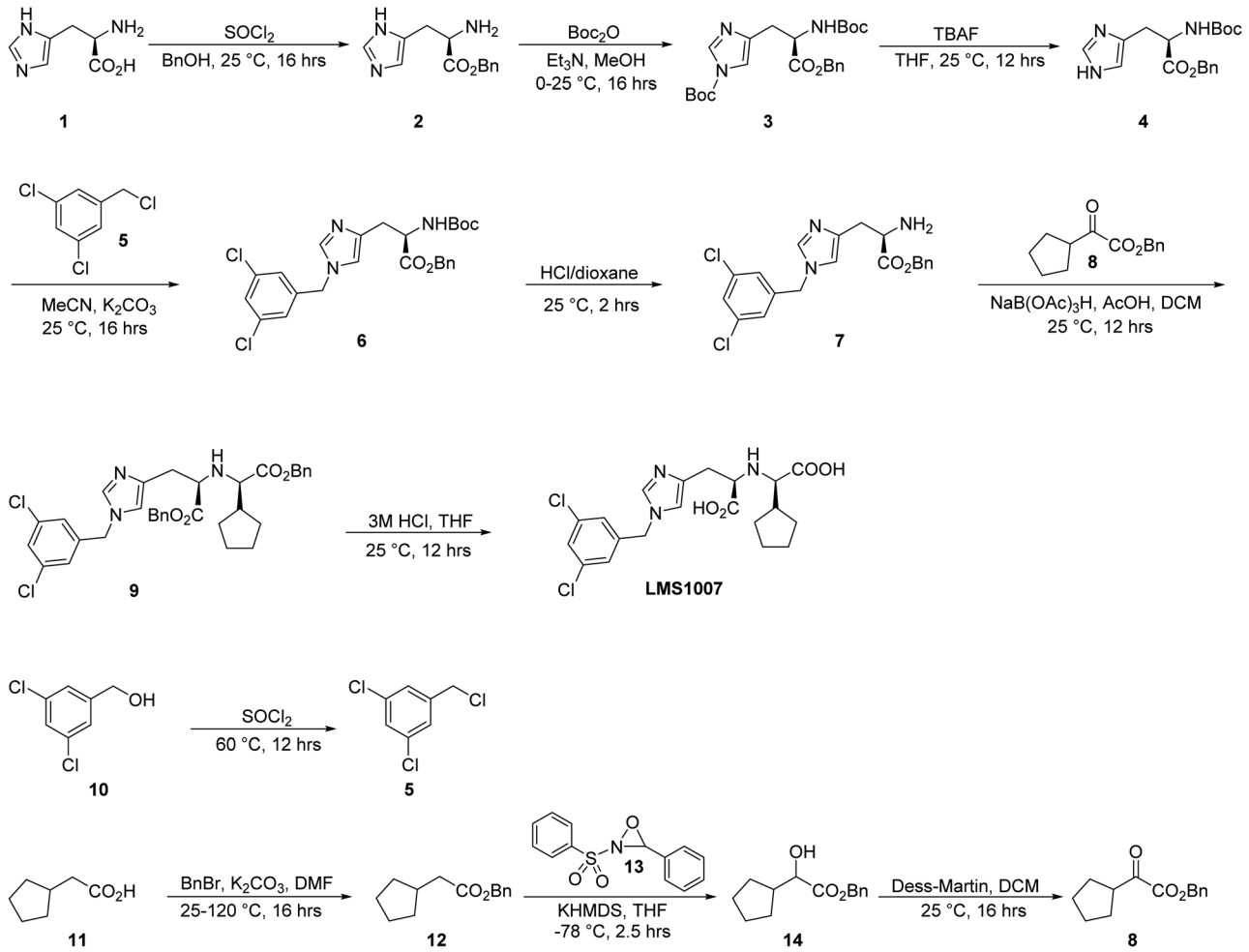

Fig. 5 The total synthesis of LMS1007.

Chemistry of LMS1007

The synthesis of **LMS1007** started with the protection of the carboxylic acid functionality in D-histidine (**1**), resulting in compound **2** (Fig. 5). Further protection of the amino group was achieved with a Boc group to afford compound **3**. The protection of the imidazole ring nitrogen was not aimed so it was deprotected in the next step using TBAF, resulting in compound **4**. The imidazole ring was then functionalized with compound **5**, which was synthesized from its commercially available corresponding alcohol derivative (**10**) to give compound **6**. Having compound **6**, the amino group deprotection was achieved using HCl/dioxane. The resulting compound (7) was functionalized with compound **8** that was obtained in three steps, as described later. The reaction resulted in a racemic mixture of the product for the new chiral center, and was then further purified by SFC to result in the required diastereomer. Finally, deprotection of the benzyl groups resulted in **LMS1007**. **LMS1007** and the synthesized intermediates were confirmed by ^{1}H-NMR and LC-MS. (All actual spectra files and graphs are available upon request).

Compound **8** was smoothly obtained from the commercially available 2-cyclopentyl acetic acid (**11**, Scheme 1). The carboxylic acid group was first protected with a benzyl group to result in compound **12**, which was functionalized on the α-carbon with a hydroxyl group using compound **13** and a base to afford compound **14**. Compound **14** was then converted to compound **8** by a reduction reaction.

Experimental validation of activities and hypotheses

LMS1007 ACE2 inhibition

LMS1007 inhibited ACE2 at doses in the range of 0.23 mM to 23.00 mM with IC_{50} of 2.27 mM. Computation of the inhibition percentage for each concentration was accomplished by calculating the ratio for the slopes of two lines. In the numerator, the slope was derived from the meticulously fitted linear equation characterizing fluorescence across five temporal points for each concentration. The denominator was the slope of the commensurate average slope associated with the enzyme control (DMSO), as delineated in Table 1. However, the inhibition exhibited a tempered character when juxtaposed with a standard inhibitor. The standard inhibitor demonstrated a more potent ACE2 inhibitory effect within a markedly lower

© 2025 The Author(s). Published by the Royal Society of Chemistry

Open Access Article. Published on 08 May 2025. Downloaded on 2/10/2026 7:24:35 PM.
This article is licensed under a Creative Commons Attribution-NonCommercial 3.0 Unported Licence.

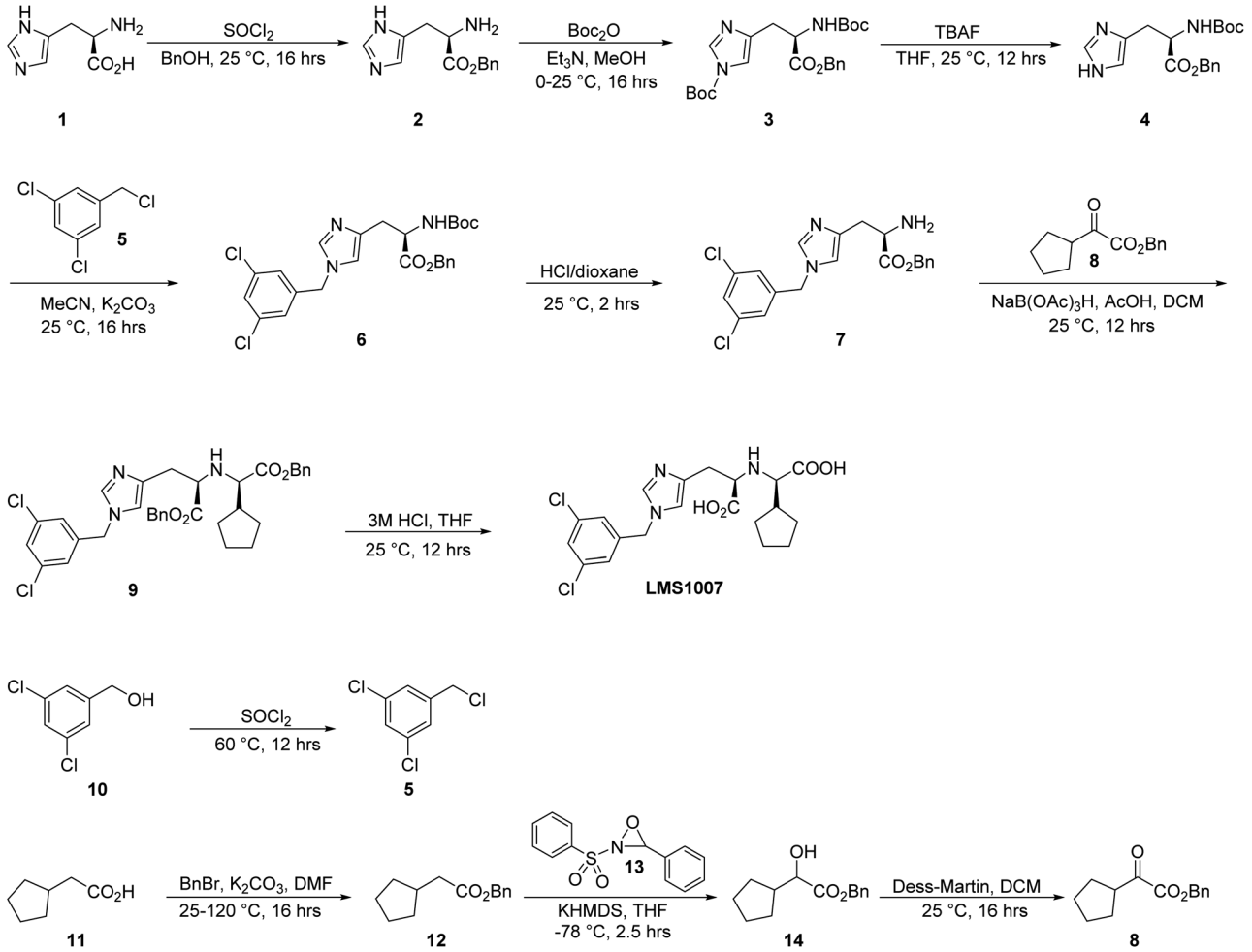

Scheme 1 The total synthesis of LMS1007.

and narrower concentration range ranging from 6.25 nM to 50 nM. On the other hand, the ACE2 inhibition was noticed at a maximum of 23 mM and a minimum of 0.23 mM. Fig. 6 panel A shows the triplicate inhibition% of both drugs at the tested concentrations. It is evident from the graph that **LMS1007** at 23 mM produces a similar ACE2 inhibition% to the standard kit inhibitor at 50 nM. Similarly, the 2.3 mM of **LMS1007** produces a similar effect to the standard kit inhibitor at 25 nM, and so on for the lower concentrations.

LMS1007 and viral spike–ACE2 inhibition kits

In the range of concentrations in Fig. 6 panel B, **LMS1007** displays similar inhibition on the SARS CoV-2 spike protein and ACE2 interaction with about the same IC_{50} of 2.3 mM. As a result, the ACE2 active site may either directly or indirectly be involved in the viral spike interaction with ACE2. However, the ACE2–spike S1 kit shows static inhibition across the whole range of concentrations. IC_{50} in this third kit is impossible to calculate.

Review and discussion

The ACE2 enzyme plays a key enzymatic role under a variety of conditions. Readers should note that the ACE2 role is ubiquitous, just like the entire renin angiotensin aldosterone systems (RAAS) that it belongs to. Most notable are the applications for ACE2 in cardiovascular and related diseases. For example, candesartan has been reported to reduce renal ubiquitination, and lysosomal degradation in male mice.[12] Growing evidence suggests that ubiquitination is the main cellular mechanism by which the host regulates the ACE2 levels in tissues, including in Covid-19 patients.[13] To elaborate a bit more on this emerging concept, ACE2 ubiquitination contributes to hypertension, but offers a new druggable target for elevated blood pressure.[14] In the latest research by Elgazzaz *et al.*,[14] the full mechanisms are reported. Therefore, according to Wang *et al.*, candesartan resulted in an upregulation of ACE2 in mice, and hence gender-differential, reno-protective and antihypertensive effect.[12] The upregulation-mediated ACE2 renoprotection has been confirmed in another rat model as well.[15] In contrast, ablation of ACE2 in rats followed by *Lactobacillus paracasei*, which were genetically engineered for the production of ACE2, has resulted in a female-rat specific reduction in the blood pressure.[16] Clinically, this renoprotection has been confirmed in 777 patients, where patients with higher ACE2 in plasma and urine had a lower progression of diabetic kidney disease and albuminuria.[17] It was suggested that the benefit of

Open Access Article. Published on 08 May 2025. Downloaded on 2/10/2026 7:24:35 PM. This article is licensed under a Creative Commons Attribution-NonCommercial 3.0 Unported Licence.

Table 1 Inhibition kit fluorescence detected at E_x/E_m = 320/420 nm for different time points (mean ± standard deviation) with the linear trendline slope[a] and inhibition% average[b] below

	Time point in minutes				
Test compound	2	17	32	47	62
LMS1007(mM)					
23	299 ± 22	365 ± 27	427 ± 33	496 ± 38	560 ± 43
	Slope = 4.4% inhibition = 96%				
2.3	3403 ± 520	4129 ± 633	4862 ± 762	5586 ± 874	6314 ± 993
	Slope = 48.5% inhibition = 50%				
0.23	6478 ± 329	7863 ± 394	9249 ± 468	10635 ± 544	12022 ± 624
	Slope = 92.4% inhibition = 6%				
0.023	6711 ± 208	8143 ± 208	9577 ± 218	11014 ± 235	12446 ± 256
	Slope = 95.6% inhibition = 2%				
0.0023	8324 ± 261	9754 ± 263	11204 ± 262	12656 ± 261	14108 ± 261
	Slope = 96.5% inhibition = 1%				
0.00023	5997 ± 545	7459 ± 508	8921 ± 475	10382 ± 442	11844 ± 410
	Slope = 97.4% inhibition = 0%				
Kit inhibitor (nM)					
50	972 ± 187	833 ± 116	952 ± 31	1027 ± 140	1072 ± 130
	Slope = 2.6% inhibition = 100%				
25	1524 ± 302	2109 ± 153	2087 ± 419	2380 ± 337	2595 ± 223
	Slope = 16.1% inhibition = 50%				
12.5	1651 ± 243	2131 ± 145	2388 ± 117	2934 ± 117	3176 ± 338
	Slope = 25.7% inhibition = 19%				
6.25	1875 ± 95	2608 ± 210	3097 ± 69	3833 ± 648	3987 ± 271
	Slope = 36.3% inhibition = 0%				
Enzyme/DMSO control[c]					
Enzyme control[a]	1876 ± 238	2407 ± 319	2836 ± 401	3363 ± 401	3792 ± 438
	Slope = 31.9% inhibition = 0%				
Enzyme control[b]	6542 ± 169	8557 ± 310	9918 ± 199	10863 ± 620	12727 ± 81
	Slope = 97.8% inhibition = 0%				

[a] Measurement sample size (n) = 3 for each time point, x is the time point and y is the fluorescence reading; actual slopes and intercepts were divided by 1000 and rounded to the nearest integer. [b] % inhibition was calculated from activity%, which was the fraction of the trendline slope to the corresponding enzyme control dilution slope. [c] DMSO is the control.

ACE2 upregulation extends to pulmonary hypertension.[18] Moreover, genetic polymorphisms in ACE2 may account for a greater probability of arterial hypertension and cardiovascular disease in systemic sclerosis patients.[19] Logically, these cardiovascular findings would generate various hypotheses to test the ACE2 role in heart failure. In fact, a study on 103 myocardial tissue samples sourced from patients in various heart failure stages have shown that ACE2 significantly increased and decreased, respectively, in cardiomyocytes and non-cardiomyocytes from heart failure stages A to C ($P < 0.001$).[20] These changes in ACE2 were associated with left ventricular remodeling in these histopathological samples. Kellum *et al.* have confirmed that these cardiac effects are especially derived from the loss of ACE2 in pericytes, suggesting that these cells are both the target of SARS CoV-2 cardiac infection and elicitor of arrhythmogenesis.[21] This active and promising research on ACE2 has triggered researchers to develop innovative models for the identification of ACE2 as a promising marker in varied pathologies, including biosensors for viral spike–ACE2.[22–24] Now, these various research articles, although they may seem confusing, point to one fact that ACE2 modulation is worth investigating, as both ACE2 inhibitors and activators may help fine-tune a variety of pathologies. Cancer is another broad group of diseases, where ACE2 seems to have important pathological roles. For example, researchers have found that ACE2 overexpression in the liver impacts the risk of fibrosis and hepatocarcinoma by inhibiting Hepatic Stellate Cell (HSC) autophagy.[25] This is mediated through the AMP-activated protein kinase (AMPK)/mammalian target of the rapamycin (mTOR) pathway. On this basis, ACE2 inhibitors, blockers, or modulators could have implications in the development and progression of liver cancer. Saadah *et al.* found that ACE2 modulation is a promising target, especially in TNBC.[6] One sole study about Kawasaki disease has shown that ACE2 was higher and correlated with lower platelet levels in this population.[26] Excluding the four SARS CoV-2 studies cited in this paragraph, we have a total of ten in Fig. 6 diseases other than SARS CoV-2. However, our query of NLM-PubMed, which returned a total of 47 articles, showed that most studies (remaining 37, 79%) were related to SARS CoV-2 and Covid-19.

Taking the Covid-19 articles, there has been only one study that found no correlation of plasma ACE2 and that it might not be a good surrogate marker of lung ACE2.[28] However, this study has provided no dynamic assessment of the ACE2 level and

 © 2025 The Author(s). Published by the Royal Society of Chemistry

Open Access Article. Published on 08 May 2025. Downloaded on 2/10/2026 7:24:35 PM.
This article is licensed under a Creative Commons Attribution-NonCommercial 3.0 Unported Licence.

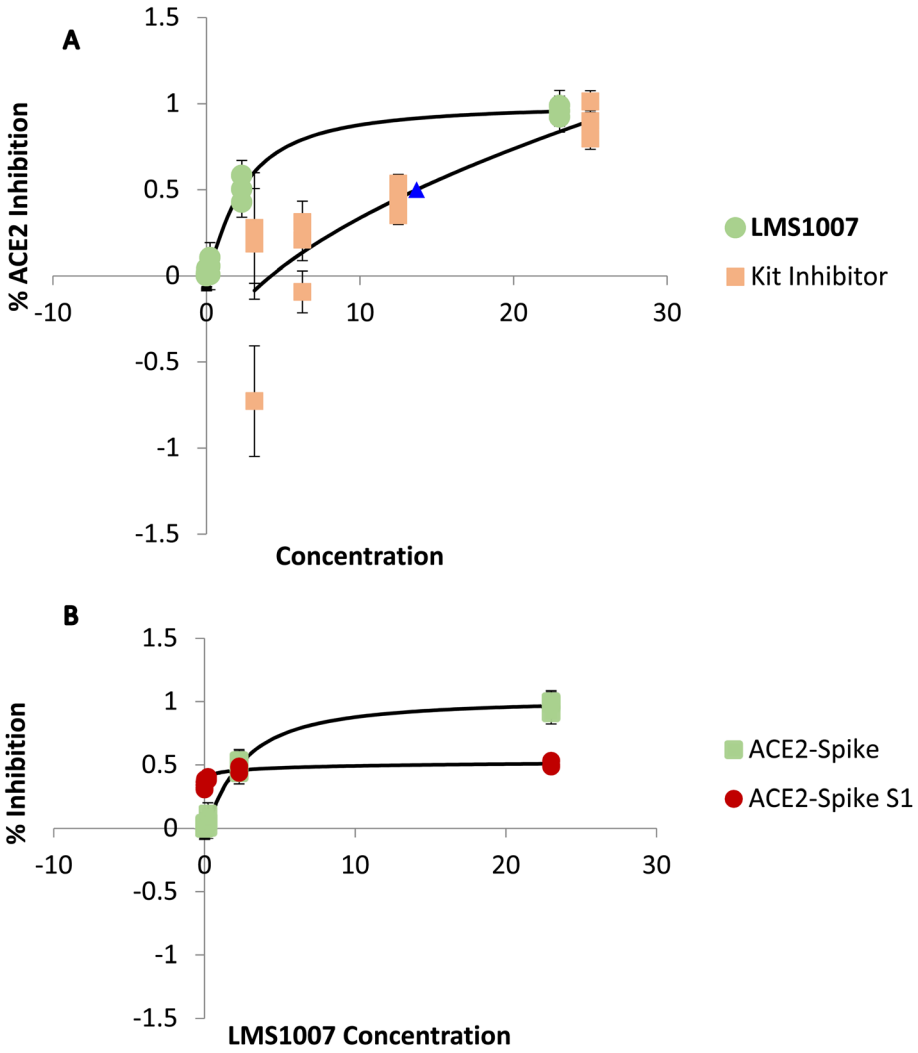

Fig. 6 Mean inhibition% of ACE2 at concentrations ranging from 0.23 μM to 23 mM for **LMS1007** and from 6.25 nm to 50 nM for the standard kit inhibitor.

activity in these different groups. Indeed, it has also found divergent changes in these levels by age, gender, and antihypertensive treatment. Additionally, other researchers have found that the wild type ACE2 has higher plasma ACE2 levels compared to other variants, and this dimension was missing in the previous study by Xie *et al.*[29] This soluble ACE2 has an important role and was protective against the aggressive Delta SARS CoV-2 for extended durations post infection.[30] Moreover, the current research direction in this area has pushed towards developing 3D-lung models that incorporate the ACE2 expression in the cells due to the consensus that this molecule is pivotal in Covid-19 lung infections.[31] Although soluble ACE2 levels are similar in SARS CoV-2 positive and negative patients, the expression levels indicated by micro RNA (miRNA), miR-141-3p, are different.[32] This means that the virus-positive patients may, in fact, respond by downregulating/upregulating ACE2. Guo *et al.* confirmed that miRNA is downregulated initially in SARS CoV-2-infected patients, and then upregulated later in the disease cycle.[33] A similar finding in ACE2 research in breast cancer has been described.[16,34–36] There, the less aggressive breast cancer cells have an initially marked reduction in the ACE2 levels compared to the normal tissues, followed by a rise in the ACE2 expression in TNBC cell lines. Moreover, higher ACE2 transcription is positively correlated with the transmission of SARS CoV-2 among hospital-admitted patients, but not healthcare providers during Covid-19 outbreaks.[37] Furthermore, the expression of ACE2 and risk of ocular SARS CoV-2 infection are higher in smokers than non-smokers.[38] In smokers, it has been also shown that washing eyes with water reduces ACE2 and SARS CoV-2 ocular infections. This concept of expression regulation is further presented in both patients with colon tissues affected by cancer and with unaffected tissues in response to SARS CoV-2 infection.[39] At other healthcare front lines, more soluble ACE2 in the brain seem to increase the risk for Alzheimer disease and other Central Nervous System (CNS) pathologies even though its relation to SARS CoV-2 CNS infection was unclear.[40] Moreover, pityriasis rosea-like lesions and other cutaneous complications have been less and of mitigated severity in Covid-19 patients with higher ACE2 expression.[41] As an extension to increased expression, multiple studies have

Open Access Article. Published on 08 May 2025. Downloaded on 2/10/2026 7:24:35 PM. This article is licensed under a Creative Commons Attribution-NonCommercial 3.0 Unported Licence.

shown that this was coupled with increased ACE2 peptidase activity.[42,43] Indeed, one of these studies has found that the increased ACE2 peptidase activity is specific to SARS CoV-2 among all other coronaviruses.[43]

The current work offers a novel approach in determining the potential active sites. These were suggested based on protein surfaces analysis based on measuring distances between the proteins. Therefore, a comparative study with the active site in others work will not be possible or applicable. Studies on the ACE2 docking are based on the defined active site that has a zinc atom, and this active site is not fully involved in the spike–ACE2 recognition. Mechanistically, the previous reports had some of the amino acids involved in the spike Receptor Binding Domain (RBD) interaction with the host ACE2, similar to our docking and chemical modeling analysis.[44,45] For example, the amino acid ASN501 has been constantly found to form H-bonding with TYR449 and ALN498 similar to the current analysis. Interrupting the RBD-ACE2 interactions subsequently inhibit various host protein interactions, which then lead to protection against SARS CoV-2 entry into host cells.[46] Additionally, SARS CoV-2 is a dynamic disease with new variants like XBB.1.5 and XBB.1.16, having novel RBD that can evade the host antibodies against the virus.[47] On the other hand, ACE2 is a highly glycated enzyme and the glycans at the C-terminus can influence its binding with viral spike.[48] In contrast de-glycosylation at other sites can improve the spike RBD-ACE2 binding.[49] This variation in the effect of de-glycosylation on viral spike RBD-ACE2 binding is perfectly in line with research that also found that SARS CoV-2 activates ACE2 in a glycosylation-independent manner.[42] Researchers have also shown that ACE2 activation is linked to its hinge-bending region, while upregulation involves various signaling pathways, transcription factors, and epigenetic modulators.[49] On the other hand, Mei *et al.* have suggested that the dual-targeting of ACE2/Neuropilin-1 (NRP1) could be a promising broad-spectrum target for treating SARS-CoV-2 emerging variants of coronavirus.[50] Accordingly, it has been recommended that future studies explore novel roles of ACE2 activators/inhibitors or up-/down-regulators in disease treatments to translate discoveries in this field to bedside applications.

Before exploring the discoveries made on the ACE2 modulators, we will cover a few more elements on this protein herein. Genetically, the G/G genotype of ACE2, rs2106809, resulted in patients that had more severe Covid-19 symptoms and adverse disease outcomes.[51] So, ACE2 genetics play a role too. Additionally, in mice, the manipulation of these genes has enabled some groups to produce new strains of mice with higher ACE2 expression and lower severity of Covid-19 mortality compared to the original mouse models.[52] Other groups have shown that Covid-19 vaccine recipients and convalescent patients had more ACE2 autoantibodies.[53] Collectively, these studies and the previous ones are consistent in increasing the demand for testing all types of ACE2 modulators on SARS CoV-2 infection and progression and in other related disease pathways.

In terms of finding ACE2 modulators and confirming the therapeutic potential in SARS CoV-2 and other related diseases, there seems to be more value to ACE2 inhibition than activation. For example, Melhem *et al.* have previously shown that carnosine is a mild ACE2 inhibitor in the range of 100–300 mM concentration. This is the same range where carnosine demonstrates broad spectrum anticancer effects, including in breast malignancies.[6] Rebelo and co-workers were able to use an ACE2 decoy, namely NL-CVX1, that mimics ACE2 and thus inhibits the spike protein recognition by the host ACE2 to interrupt the viral spread.[54] Yet, in their study, the decoy-exposed patients still made SARS CoV-2 antibodies and memory T cells. Most other investigations have focused on preventing the spike–ACE2 interaction. For example, Pashameah and colleagues have discovered raffinose sulfate inhibitory effects on spike–ACE2 with no effect for the drug on ACE2 peptidase activity.[55] This inhibitory effect is coupled with an improved tolerability compared to other sulfated polysaccharides, *e.g.*, heparin and heparan. Luteolin also has inhibitory effects on spike–ACE2 binding.[56] As a result, luteolin has been shown to be associated with less platelet aggregation and thrombosis. This link between ACE2 and platelet spread and aggregation in Covid-19 patients has been confirmed by another group.[57] In another study, natural herbal medicine Eunkyo-san diminishes the levels of both inflammatory cytokines and ACE2, and may therefore help in mitigating the cytokine storm of Covid-19.[58] Biscoumarin glycosides from *P. trimera* roots hold potential as natural ACE-2 inhibitors for preventing SARS-CoV-2 infection both *in silico* and *in vitro*.[59] One of the very first drugs that were repurposed for Covid-19 is hydroxychloroquine, and findings showed that only the (*S*)-(+) enantiomer inhibits ACE2 in comparison to the (*R*)-(−) enantiomer.[60] However, data have shown that ursodeoxycholic acid prevents both the Delta and Omicron variants of SARS CoV-2 infection in hamster models.[61] More ACE2 inhibitors are on the way as well, with Harman *et al.* proposing the most potent ACE2 inhibitors *in vitro*, a group of constrained bicyclic peptides, as candidates for SARS CoV-2 infection management.[62] Studies conducted by our research teams, including the current one, have shown a clear match of ACE2 inhibition and *in vitro* effects in two diseases, triple negative cell line proliferation and SARS CoV-2–host interaction. Current work adds further evidence that ACE2 inhibition at the active site indirectly interfere with ACE2–spike interaction in a manner independent of the spike S1 unit responsible for this coupling by the two proteins. Therefore, future studies must further elaborate on the possible mechanisms of how this ACE2 inhibition possibly induces conformational changes that prevent the host–viral proteins interaction. These results weigh on adding more research efforts into exploring the role of ACE2 in these and other diseases. More potent ACE2 and potent direct ACE2–spike S1 inhibitors must be tested as well. Among the various inhibitors, ORE-1001 (aka MLN-4760) is the most potent. However, clinical applications of this drug were challenged owing to the diverse effects that it had. The current clinical status of this molecule involves the use radiofluorine derivatives for PET imaging and crystallography to further understand the role it has in human disease.[63] Thus, the current research may help to fully elicit the complexity of the ACE2 role, hence facilitating the development of selective and disease-specific ACE2 inhibitors.

© 2025 The Author(s). Published by the Royal Society of Chemistry

Open Access Article. Published on 08 May 2025. Downloaded on 2/10/2026 7:24:35 PM.
This article is licensed under a Creative Commons Attribution-NonCommercial 3.0 Unported Licence.

Conclusion

The scientific drug discovery community is progressively working toward the development of ACE2 or ACE2–spike inhibitors. However, despite the limited *in vitro* and *in vivo* proofs of this concept, a full picture of the inhibition of ACE2 is still missing, in addition to its role in preventing SARS CoV-2 infection. The current analysis has added a few pieces to the puzzle. **LMS1007**, the novel mild ACE2 inhibitor, was 100 times more potent than carnosine. Both showed activity on two different diseases in their same respective range of ACE2 inhibitions. Carnosine was effective against TNBC at an IC_{50} of about 230 mM.[6] Meanwhile, **LMS1007** was effective in inhibiting SARS CoV-2 spike ACE2 interaction at an IC_{50} of 2.3 mM. Future experiments should scale up the validation of ACE2 as a target for drug therapy in Covid-19 and TNBC. More research is needed on the myriads of effects for the ACE2 inhibition in the mesh of diseases affected by this novel and key enzyme. These diseases include a variety of cancers, neurodegenerative, autoimmune, and infectious diseases. Both carnosine and **LMS1007** are potential ACE2 inhibitor leads for anti-cancer treatment and for combating Covid-19.

Abbreviations

ACE2	Angiotensin converting enzyme 2
Covid-19	Novel coronavirus disease of 2019
SARS CoV-2	Severe acute respiratory syndrome corona virus 2
SBDD	Structure-based drug docking
TNBC	Triple negative breast cancer

Data availability

Datasets are provided as a ESI EXCEL file.† Spectra files and graphs of **LMS1007** are available as a ESI file.† All other intermediate compound spectrum files and graphs are available from the corresponding author upon reasonable request.

Author contributions

All the authors contributed to the conceptualization and writing of this research. LS performed the initial design, *in silico* testing, preliminary docking, secured funds, registered a patent, and finally experimentally validated **LMS1007**. GA proposed the synthetic routes, managed the synthesis and characterization of **LMS1007**, and contributed to the writing and analysis of the data. QA carried out the detailed docking and chemical modeling, prepared all the figures pertaining to the specific amino acids at the target sites, and contributed to the writing and analysis of the data. IB supervised the project and coordinated all efforts and contributed to the writing and analysis of the data.

Conflicts of interest

The authors have no competing interests to disclose.

Acknowledgements

L. S. secured funding for this project from Applied Science Private University # DRGS-2021-2022-6. The authors would like to thank Applied Science Private University for their kind funding for this research with the grant number DRGS-2021-2022-6.

References

1 H. Vatansev, C. Kadiyoran, M. Cumhur Cure and E. Cure, COVID-19 infection can cause chemotherapy resistance development in patients with breast cancer and tamoxifen may cause susceptibility to COVID-19 infection, *Med. Hypotheses*, 2020, **143**, 110091, DOI: 10.1016/j.mehy.2020.110091.

2 C. F. Yang, C. C. Liao, H. W. Hsu, *et al.*, Human ACE2 protein is a molecular switch controlling the mode of SARS-CoV-2 transmission, *J. Biomed. Sci.*, 2023, **30**(1), 87, DOI: 10.1186/s12929-023-00980-w.

3 V. Bezzerri, V. Gentili, M. Api, *et al.*, SARS-CoV-2 viral entry and replication is impaired in Cystic Fibrosis airways due to ACE2 downregulation, *Nat. Commun.*, 2023, **14**(1), 132, DOI: 10.1038/s41467-023-35862-0.

4 S. J. L. Petitjean, S. Eeckhout, M. Delguste, Q. Zhang, K. Durlet and D. Alsteens, Heparin-Induced Allosteric Changes in SARS-CoV-2 Spike Protein Facilitate ACE2 Binding and Viral Entry, *Nano Lett.*, 2023, **23**(24), 11678–11684, DOI: 10.1021/acs.nanolett.3c03550.

5 L. M. Saadah, G. I. A. Deiab, Q. Al-Balas and I. A. Basheti, Carnosine to Combat Novel Coronavirus (nCoV): Molecular Docking and Modeling to Cocrystallized Host Angiotensin-Converting Enzyme 2 (ACE2) and Viral Spike Protein, *Molecules*, 2020, **25**(23), 5605, DOI: 10.3390/molecules25235605.

6 S. A. Melhem, L. M. Saadah, Z. S. Attallah, I. A. Mansi, S. H. Hamed and W. H. Talib, Deciphering angiotensin converting enzyme 2 (ACE2) inhibition dynamics: Carnosine's modulatory role in breast cancer proliferation - A clinical sciences perspective, *Heliyon*, 2024, **10**(19), e38685, DOI: 10.1016/j.heliyon.2024.e38685.

7 P. M. E. Gaafar, N. S. El-Salamouni, R. M. Farid, H. A. Hazzah, M. W. Helmy and O. Y. Abdallah, Pegylated liquisomes: A novel combined passive targeting nanoplatform of L-carnosine for breast cancer, *Int. J. Pharm.*, 2021, **602**, 120666, DOI: 10.1016/j.ijpharm.2021.120666.

8 R. M. Farid, P. M. E. Gaafar, H. A. Hazzah, M. W. Helmy and O. Y. Abdallah, Chemotherapeutic potential of L-carnosine from stimuli-responsive magnetic nanoparticles against breast cancer model, *Nanomedicine*, 2020, **15**(9), 891–911, DOI: 10.2217/nnm-2019-0428.

9 R. Fatehi, M. Nouraei, M. Panahiyan, M. Rashedinia and N. Firouzabadi, Modulation of ACE2/Ang1-7/Mas and ACE/AngII/AT1 axes affects anticancer properties of sertraline in MCF-7 breast cancer cells, *Biochem. Biophys. Rep.*, 2024, **38**, 101738, DOI: 10.1016/j.bbrep.2024.101738.

Open Access Article. Published on 08 May 2025. Downloaded on 2/10/2026 7:24:35 PM. This article is licensed under a Creative Commons Attribution-NonCommercial 3.0 Unported Licence.

10 L. Saadah, G. Abu Deiab, I. Basheti and Q. Al-Balas, Compounds and Pharmaceutical Compositions for Treating Coronavirus Disease and Methods of Preparation Thereof, WO2023238167, Worldwide, 2023. C07.

11 J. Lan, J. Ge, J. Yu, *et al.*, Structure of the SARS-CoV-2 spike receptor-binding domain bound to the ACE2 receptor, *Nature*, 2020, **581**(7807), 215–220, DOI: **10.1038/s41586-020-2180-5**.

12 P. Wang, Z. Ren, W. Wang, *et al.*, Candesartan upregulates angiotensin-converting enzyme 2 in kidneys of male animals by decreased ubiquitination, *FASEB J.*, 2024, **38**(6), e23537, DOI: **10.1096/fj.202302707R**.

13 M. Elgazzaz, C. M. Filipeanu and E. Lazartigues, Angiotensin-Converting Enzyme 2 Posttranslational Modifications and Implications for Hypertension and SARS-CoV-2: 2023 Lewis K. Dahl Memorial Lecture, *Hypertension*, 2024, **81**(7), 1438–1449, DOI: **10.1161/HYPERTENSIONAHA.124.22067**.

14 M. Elgazzaz, N. Lakkappa, C. Berdasco, *et al.*, UBR1 Promotes Sex-Dependent ACE2 Ubiquitination in Hypertension, *Hypertension*, 2025, **82**(1), 84–95, DOI: **10.1161/HYPERTENSIONAHA.124.23196**.

15 A. M. Sanad, F. Qadri, E. Popova, *et al.*, Transgenic angiotensin-converting enzyme 2 overexpression in the rat vasculature protects kidneys from ageing-induced injury, *Kidney Int.*, 2023, **104**(2), 293–304, DOI: **10.1016/j.kint.2023.04.007**.

16 X. Mei, B. Mell, S. Aryal, *et al.*, Genetically engineered Lactobacillus paracasei rescues colonic angiotensin converting enzyme 2 (ACE2) and attenuates hypertension in female Ace2 knock out rats, *Pharmacol. Res.*, 2023, **196**, 106920, DOI: **10.1016/j.phrs.2023.106920**.

17 A. Ueno, Y. Onishi, K. Mise, *et al.*, Plasma angiotensin-converting enzyme 2 (ACE2) is a marker for renal outcome of diabetic kidney disease (DKD) (U-CARE study 3), *BMJ Open Diabetes Res. Care.*, 2024, **12**(3), e004237, DOI: **10.1136/bmjdrc-2024-004237**.

18 K. A. Papavassiliou, V. A. Gogou and A. G. Papavassiliou, Angiotensin-Converting Enzyme 2 (ACE2) Signaling in Pulmonary Arterial Hypertension: Underpinning Mechanisms and Potential Targeting Strategies, *Int. J. Mol. Sci.*, 2023, **24**(24), 17441, DOI: **10.3390/ijms242417441**.

19 B. Miziołek, C. Kruszniewska-Rajs, J. Gola, *et al.*, Correlation between angiotensin-converting-enzyme 2 gene polymorphisms and systemic sclerosis, *Clin. Exp. Rheumatol.*, 2023, **41**(8), 1652–1658, DOI: **10.55563/clinexprheumatol/utmjnq**.

20 V. Siratavičiūtė, D. Pangonytė, L. Utkienė, *et al.*, Myocardial Angiotensin-Converting Enzyme 2 Protein Expression in Ischemic Heart Failure, *Int. J. Mol. Sci.*, 2023, **24**(24), 17145, DOI: **10.3390/ijms242417145**.

21 C. L. Kellum, L. G. Kirkland, T. K. Nelson, *et al.*, Sympathetic remodeling and altered angiotensin-converting enzyme 2 localization occur in patients with cardiac disease but are not exacerbated by severe COVID-19, *Auton. Neurosci.*, 2024, **251**, 103134, DOI: **10.1016/j.autneu.2023.103134**.

22 Y. Liu, Y. He, G. Zhang, J. Yang and Y. Li, Multifunctional Self-Signaling nanoMIP and Its Application for a Washing-Free Assay of Human Angiotensin-Converting Enzyme 2, *Anal. Chem.*, 2024, **96**(19), 7602–7608, DOI: **10.1021/acs.analchem.4c00501**.

23 S. Karthikeyan, A. Sundaramoorthy, S. Kandasamy, *et al.*, A biophysical approach of tyrphostin AG879 binding information in: bovine serum albumin, human ErbB2, c-RAF1 kinase, SARS-CoV-2 main protease and angiotensin-converting enzyme 2, *J. Biomol. Struct. Dyn.*, 2024, **42**(3), 1455–1468, DOI: **10.1080/07391102.2023.2204368**.

24 (*a*) Y. Yang, J. Cui, D. Luo, *et al.*, Rapid Detection of SARS-CoV-2 Variants Using an Angiotensin-Converting Enzyme 2-Based Surface-Enhanced Raman Spectroscopy Sensor Enhanced by CoVari Deep Learning Algorithms. *ACS Sens.*. **9**(6):3158–3169. doi:DOI: **10.1021/acssensors.4c00488**; (*b*) J. Xie, Q. F. Huang, Z. Zhang, *et al.*, Angiotensin-converting enzyme 2 in human plasma and lung tissue, *Blood Press.*, 2023, **32**(1), 6–15, DOI: **10.1080/08037051.2022.2154745**.

25 M. Barone, Angiotensin-converting enzyme 2 and AMPK/mTOR pathway in the treatment of liver fibrosis: Should we consider further implications?, *World J. Gastroenterol.*, 2024, **30**(18), 2391–2396, DOI: **10.3748/wjg.v30.i18.2391**.

26 Y. Gan, Y. Feng, X. Zhou, *et al.*, Serum levels of angiotensin-converting enzyme 2 in children with Kawasaki disease, *Clin. Exp. Med.*, 2023, **23**(4), 1325–1330, DOI: **10.1007/s10238-022-00933-x**.

27 N. Naderi and M. Rahimzadeh, The Role of Soluble ACE2 as a Prognostic Marker in Severe COVID-19: A Brief Meta-Analysis, *Endocr., Metab. Immune Disord.:Drug Targets*, 2023, **23**(1), 70–76, DOI: **10.2174/1871530322666220623121922**.

28 J. Xie, Q. F. Huang, Z. Zhang, *et al.*, Angiotensin-converting enzyme 2 in human plasma and lung tissue, *Blood Press.*, 2023, **32**(1), 6–15, DOI: **10.1080/08037051.2022.2154745**.

29 R. Ahmed, A. A. Saba, A. Paul, *et al.*, Intronic Variants of the Angiotensin-Converting Enzyme 2 Gene Modulate Plasma ACE2 Levels and Possibly Confer Protection against Severe COVID-19, *BioMed Res. Int.*, 2023, **2023**, 5705076, DOI: **10.1155/2023/5705076**.

30 C. Cianfarini, L. Hassler, J. Wysocki, *et al.*, Soluble Angiotensin-Converting Enzyme 2 Protein Improves Survival and Lowers Viral Titers in Lethal Mouse Model of Severe Acute Respiratory Syndrome Coronavirus Type 2 Infection with the Delta Variant, *Cells*, 2024, **13**(3), 203, DOI: **10.3390/cells13030203**.

31 J. F. Dos Santos, E. M. Dos Reis, F. V. Berti, G. Colla, J. Koepp and V. A. Nunes, CALU-3 lung cells three-dimensionally assembled onto CellFate® matrix present angiotensin-converting enzyme-2 activity, *Biotechnol. Bioeng.*, 2023, **120**(12), 3602–3611, DOI: **10.1002/bit.28552**.

32 E. Kakavandi, K. Sadeghi, M. Shayestehpour, *et al.*, Evaluation of angiotensin converting enzyme 2 (ACE2), angiotensin II (Ang II), miR-141-3p, and miR-421 levels in SARS-CoV-2 patients: a case-control study, *BMC Infect. Dis.*, 2024, **24**(1), 429, DOI: **10.1186/s12879-024-09310-3**.

© 2025 The Author(s). Published by the Royal Society of Chemistry

Open Access Article. Published on 08 May 2025. Downloaded on 2/10/2026 7:24:35 PM. This article is licensed under a Creative Commons Attribution-NonCommercial 3.0 Unported Licence.

33 N. Guo, X. Li, Z. Han, *et al.*, Expression of angiotensin converting enzyme 2 mRNA in different SARS-CoV-2 infection states and times, *J. Biomol. Struct. Dyn.*, 2023, **41**(20), 11255–11261, DOI: 10.1080/07391102.2022.2160821.

34 H. S. Parmar, A. Nayak, P. K. Gavel, H. C. Jha, S. Bhagwat and R. Sharma, Cross Talk between COVID-19 and Breast Cancer, *Curr. Cancer Drug Targets*, 2021, **21**(7), 575–600, DOI: 10.2174/1568009621666210216102236.

35 V. K. Bhari, D. Kumar, S. Kumar and R. Mishra, SARS-CoV-2 cell receptor gene ACE2 -mediated immunomodulation in breast cancer subtypes, *Biochem. Biophys. Rep.*, 2020, **24**, 100844, DOI: 10.1016/j.bbrep.2020.100844.

36 M. G. Nair, J. S. Prabhu and S. Ts, High expression of ACE2 in HER2 subtype of breast cancer is a marker of poor prognosis, *Cancer Treat Res Commun.*, 2021, **27**, 100321, DOI: 10.1016/j.ctarc.2021.100321.

37 A. M. Nikiforuk, K. S. Kuchinski, K. Short, *et al.*, Nasopharyngeal angiotensin converting enzyme 2 (ACE2) expression as a risk-factor for SARS-CoV-2 transmission in concurrent hospital associated outbreaks, *BMC Infect. Dis.*, 2024, **24**(1), 262, DOI: 10.1186/s12879-024-09067-9.

38 H. Fujishima, H. Yazu, E. Shimizu, N. Okada and K. Fukagawa, Eye Washing Downregulated Angiotensin-Converting Enzyme 2 in Conjunctival Tissue Samples from Smokers, *Int. J. Mol. Sci.*, 2023, **24**(24), 17526, DOI: 10.3390/ijms242417526.

39 M. A. Alotaibi, T. M. I. Al-Hazani, M. A. Alwaili, *et al.*, SARS-CoV-2 virus associated angiotensin converting enzyme 2 expression modulation in colorectal cancer: Insights from mRNA and protein analysis COVID-19 associated (ACE2) expression in colorectal cancer, *Microb. Pathog.*, 2023, **185**, 106389, DOI: 10.1016/j.micpath.2023.106389.

40 L. Reveret, M. Leclerc, V. Emond, *et al.*, Higher angiotensin-converting enzyme 2 (ACE2) levels in the brain of individuals with Alzheimer's disease, *Acta Neuropathol. Commun.*, 2023, **11**, 173.

41 A. G. Abdou, M. Fayed and A. G. A. Farag, Immunohistochemical Expression of Angiotensin-Converting Enzyme 2 in the Skin of Patients Affected by COVID-19, *Am. J. Dermatopathol.*, 2024, **46**(1), 1–13, DOI: 10.1097/DAD.0000000000002498.

42 X. A. Mendiola-Salazar, M. A. Munguía-Laguna, M. Franco, A. Cano-Martínez, J. Santamaría Sosa and R. Bautista-Pérez, SARS-CoV-2 Spike Protein Enhances Carboxypeptidase Activity of Angiotensin-Converting Enzyme 2, *Int. J. Mol. Sci.*, 2024, **25**(11), 6276, DOI: 10.3390/ijms25116276.

43 J. Bejoy, C. I. Williams, H. J. Cole, *et al.*, Effects of spike proteins on angiotensin converting enzyme 2 (ACE2), *Arch. Biochem. Biophys.*, 2023, **748**, 109769, DOI: 10.1016/j.abb.2023.109769.

44 I. Biskupek and A. Gieldon, Two-Stage Recognition Mechanism of the SARS-CoV-2 Receptor-Binding Domain to Angiotensin-Converting Enzyme-2 (ACE2), *Int. J. Mol. Sci.*, 2024, **25**(1), 679, DOI: 10.3390/ijms25010679.

45 C. Peng, X. Lv, Z. Zhang, J. Lin and D. Li, The Recognition Pathway of the SARS-CoV-2 Spike Receptor-Binding Domain to Human Angiotensin-Converting Enzyme 2, *Molecules*, 2024, **29**(8), 1875, DOI: 10.3390/molecules29081875.

46 S. Karthikeyan, A. Sundaramoorthy, S. Kandasamy, *et al.*, A biophysical approach of tyrphostin AG879 binding information in: bovine serum albumin, human ErbB2, c-RAF1 kinase, SARS-CoV-2 main protease and angiotensin-converting enzyme 2, *J. Biomol. Struct. Dyn.*, 2024, **42**(3), 1455–1468, DOI: 10.1080/07391102.2023.2204368.

47 T. Sharma, B. Gerstman and P. Chapagain, Distinctive Features of the XBB.1.5 and XBB.1.16 Spike Protein Receptor-Binding Domains and Their Roles in Conformational Changes and Angiotensin-Converting Enzyme 2 Binding, *Int. J. Mol. Sci.*, 2023, **24**(16), 12586, DOI: 10.3390/ijms241612586.

48 L. Wei, Y. Chen, X. Feng, *et al.*, Elucidation of N-/O-glycosylation and site-specific mapping of sialic acid linkage isomers of SARS-CoV-2 human receptor angiotensin-converting enzyme 2, *Analyst*, 2023, **148**(20), 5002–5011, DOI: 10.1039/d3an01079a.

49 Y. Zhou, C. Tan and R. Zenobi, Rapid Profiling of the Glycosylation Effects on the Binding of SARS-CoV-2 Spike Protein to Angiotensin-Converting Enzyme 2 Using MALDI-MS with High Mass Detection, *Anal. Chem.*, 2024, **96**(5), 1898–1905, DOI: 10.1021/acs.analchem.3c03930.

50 S. Mei, Y. Zou, S. Jiang, *et al.*, Highly potent dual-targeting angiotensin-converting enzyme 2 (ACE2) and Neuropilin-1 (NRP1) peptides: A promising broad-spectrum therapeutic strategy against SARS-CoV-2 infection, *Eur. J. Med. Chem.*, 2024, **263**, 115908, DOI: 10.1016/j.ejmech.2023.115908.

51 H. Mohammadi-Berenjestanaki, E. Mohammadali, M. Khasayesi, *et al.*, Association between angiotensin-converting enzyme-2 gene polymorphism (rs2106809) with severity and outcome of COVID-19 infection, *Mol. Biol. Rep.*, 2023, **50**(8), 6669–6679, DOI: 10.1007/s11033-023-08493-3.

52 C. M. Bradshaw, T. Georgieva, T. N. Tankersley, *et al.*, Cutting Edge: Characterization of Low Copy Number Human Angiotensin-Converting Enzyme 2-Transgenic Mice as an Improved Model of SARS-CoV-2 Infection, *J. Immunol.*, 2024, **212**(4), 523–528, DOI: 10.4049/jimmunol.2300591.

53 J. Y. H. Tsoi, J. Cai, J. Situ, *et al.*, Autoantibodies against angiotensin-converting enzyme 2 (ACE2) after COVID-19 infection or vaccination, *J. Med. Virol.*, 2023, **95**(12), e29313, DOI: 10.1002/jmv.29313.

54 M. Rebelo, C. Tang, A. R. Coelho, *et al.*, De Novo Human Angiotensin-Converting Enzyme 2 Decoy NL-CVX1 Protects Mice From Severe Disease After Severe Acute Respiratory Syndrome Coronavirus 2 Infection, *J. Infect. Dis.*, 2023, **228**(6), 723–733, DOI: 10.1093/infdis/jiad135.

55 R. A. Pashameah, R. Soltane and A. M. Sayed, Discovery of raffinose sulfate as a potential SARS CoV-2 inhibitor *via* blocking its binding with angiotensin converting enzyme 2, *Int. J. Biol. Macromol.*, 2023, **248**, 125818, DOI: 10.1016/j.ijbiomac.2023.125818.

Open Access Article. Published on 08 May 2025. Downloaded on 2/10/2026 7:24:35 PM.
This article is licensed under a Creative Commons Attribution-NonCommercial 3.0 Unported Licence.

56 J. Zhu, H. Yan, M. Shi, *et al.*, Luteolin inhibits spike protein of severe acute respiratory syndrome coronavirus-2 (SARS-CoV-2) binding to angiotensin-converting enzyme 2, *Phytother. Res.*, 2023, **37**(8), 3508–3521, DOI: **10.1002/ptr.7826**.

57 H. A. Waggiallah, M. M. Eltayeb, A. M. Hjazi and Y. M. Elmosaad, High expression of angiotensin-converting enzyme 2 receptor (ACE-2), transmembrane protease serine (TMPRSS), and P-selectin in platelets lead to thrombosis formation in COVID-19 patients, *Eur. Rev. Med. Pharmacol. Sci.*, 2024, **28**(5), 1847–1856, DOI: **10.26355/eurrev_202403_35598**.

58 H. Y. Kim, K. M. Jeong, S. H. Kim, *et al.*, Modulating effect of Eunkyo-san on expression of inflammatory cytokines and angiotensin-converting enzyme 2 in human mast cells, *In Vitro Cell. Dev. Biol.: Anim.*, 2024, **60**(2), 195–208, DOI: **10.1007/s11626-024-00847-w**.

59 N. X. Ha, T. T. Huong, P. N. Khanh, *et al.*, *In vitro* and in Silico Study of New Biscoumarin Glycosides from Paramignya trimera against Angiotensin-Converting Enzyme 2 (ACE-2) for Preventing SARS-CoV-2 Infection, *Chem. Pharm. Bull.*, 2024, **72**(6), 574–583, DOI: **10.1248/cpb.c23-00844**.

60 F. Aiello, F. Balzano, G. Uccello Barretta, I. D'Acquarica, G. Mazzoccanti and I. Agranat, Chiral distinction between hydroxychloroquine enantiomers in binding to angiotensin-converting enzyme 2, the forward receptor of SARS-CoV-2, *J. Pharm. Biomed. Anal.*, 2024, **237**, 115770, DOI: **10.1016/j.jpba.2023.115770**.

61 K. Lee, Y. Na, M. Kim, *et al.*, Ursodeoxycholic acid may protect from severe acute respiratory syndrome coronavirus 2 Omicron variant by reducing angiotensin-converting enzyme 2, *Pharmacol. Res. Perspect.*, 2024, **12**(2), e1194, DOI: **10.1002/prp2.1194**.

62 M. A. J. Harman, S. J. Stanway, H. Scott, *et al.*, Structure-Guided Chemical Optimization of Bicyclic Peptide (Bicycle) Inhibitors of Angiotensin-Converting Enzyme 2, *J. Med. Chem.*, 2023, **66**(14), 9881–9893, DOI: **10.1021/acs.jmedchem.3c00710**.

63 J. Wang, D. Beyer, C. Vaccarin, *et al.*, Development of radiofluorinated MLN-4760 derivatives for PET imaging of the SARS-CoV-2 entry receptor ACE2, *Eur. J. Nucl. Med. Mol. Imaging*, 2024, **52**(1), 9–21, DOI: **10.1007/s00259-024-06831-6**.

© 2025 The Author(s). Published by the Royal Society of Chemistry